CHAPTER 3

Design, Synthesis and Biological Evaluation of Thioacetamide-linked 1,3,4-Thiadiazole-2-Amines

3. Thioacetamide-linked 1,3,4-thiadiazole-2-amines (STS series)

3.1. Design rationale and plan of work

3.1.1. Design rationale

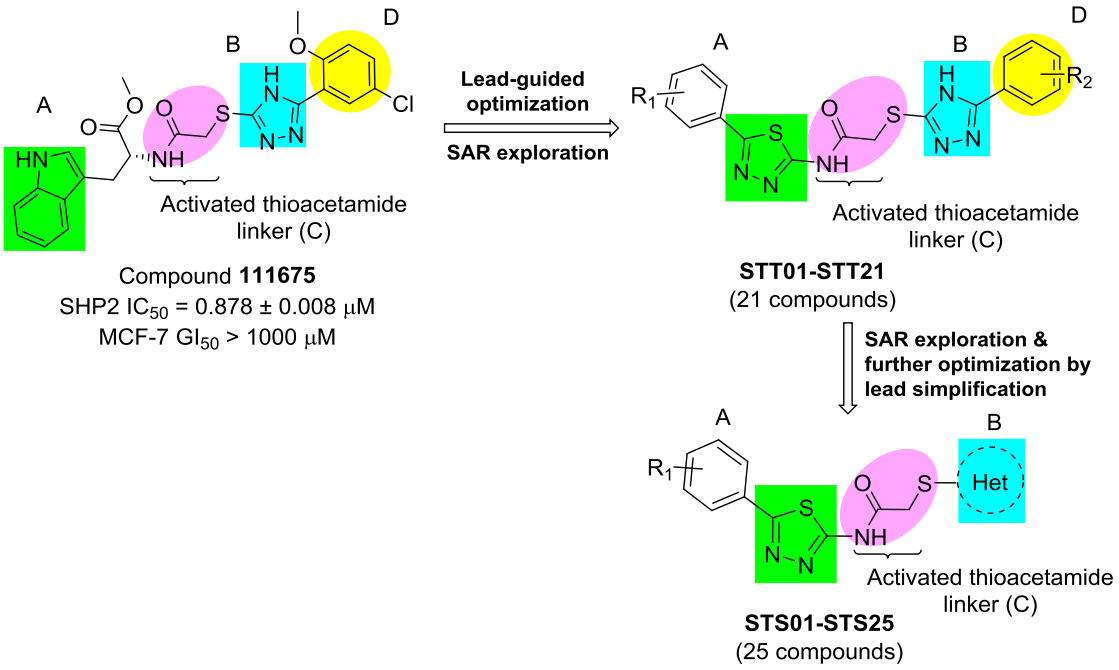

Figure 3.1. Design rationale of compounds **STS01-STS25**

With our current objective to further optimize the previous series of compounds i.e., **STT series** to further improve the resultant SHP2 inhibitory potential, the few rational modifications were made on the general structure of **STT series** by an approach of lead simplification (**Figure 3.1**). This was formulated by replacement of the aryl/heteroaryl system of **STT** structure with simple or benzene-fused five membered heterocyclic

systems in order to optimize the size of the lipophilic ring responsible for SHP2 inhibitory activity.

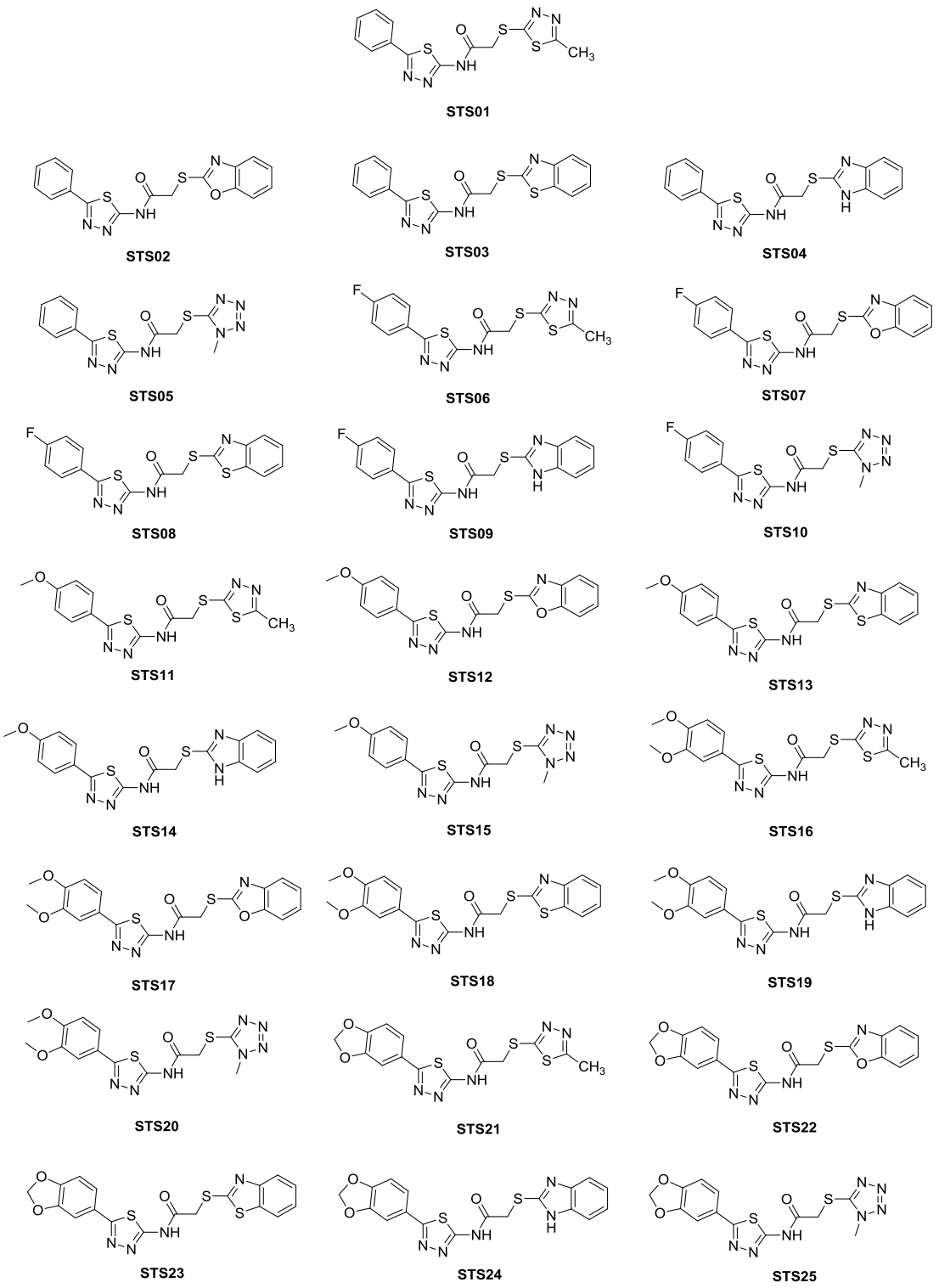

Figure 3.2. Skeletal formulae of rationally designed compounds (**STS01-STS25**)

The following changes were attempted; i) retention of phenyl substituted 1,3,4-thiadiazole (**A**) as one of the main variable centre to maintain flexibility and binding, and ii) replacement of second heterocyclic complex i.e. phenyl substituted 1,2,4-triazole (**B** & **D)** with simpler heterocyclic systems like 1,3,4-thiadiazole (an ostensible homodimer), tetrazole ring etc. or benzene-fused heterocycles like benzothiazole, benzimidazole etc.

Thus, the final structure of the **STS series** is a thioacetamide of various simple or benzene-fused 5-membered heterocyclic thiols with 5-phenyl-1,3,4-thiadiazole-2-amine (**Figure 3.2**).

3.1.2. Plan of work

The plan of work for the design and development of the current series of compounds (**STS01-STS25**) is represented schematically in **Figure 3.3**. Lead-guided optimization via structural simplification was applied to design and synthesize a set of new analogous molecules which were subsequently evaluated biologically by *in vitro, in cellulo, in vivo* and *ex vivo* studies for desired efficacy and undesired toxicity.

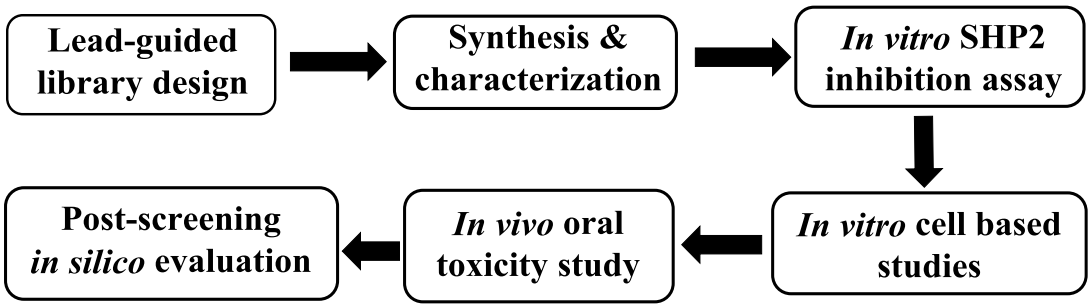

Figure 3.3. Schematic workflow for plan of work

3.2. Experimental work

3.2.1. Chemistry

3.2.1.1. Synthesis of compounds STS01-STS25

Laboratory grade synthetic reagents were procured from Sigma-Aldrich Chemical Private Ltd., India, Merck India, Fischer Scientific Ltd., Central Drug House (P) Ltd. India, Loba Chemie India, Sisco Research Laboratories Pvt Ltd., India etc. and used as such without further purification. In general, reaction was monitored by TLC with the help of pre-coated silica gel plates (Merck, Kieselgel 60F-254, 0.20 mm).

Step 1 & 2: Synthetic procedure for fragments TDZ01-TDZ05 and TDZA01-TDZA05

Synthesis of fragments **TDZ01-TDZ05** and **TDZA01-TDZA05** has been mentioned earlier under **Scheme 2.1** and the same intermediates have been used for the synthesis of compounds **STS01-STS25** by method mentioned below.

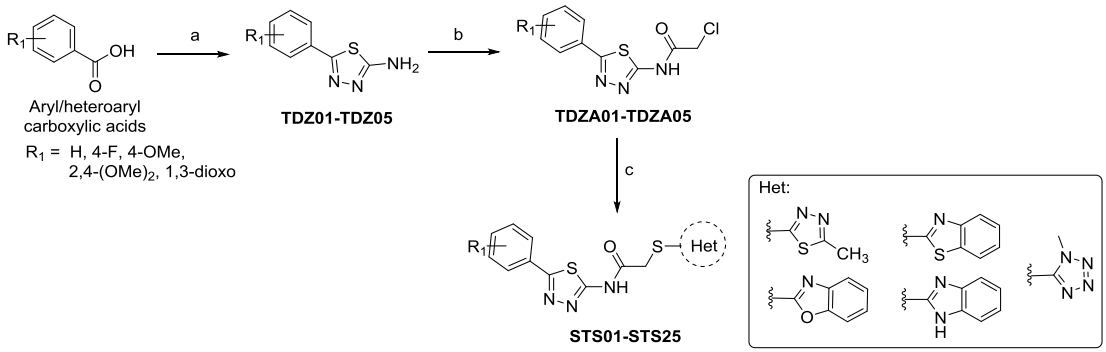

Scheme 3.1. Synthetic scheme for compounds **STS01-STS25.** *Reagents & conditions*: (a) i) thiosemicarbazide, $POCl_3$, 75-80 ºC, 0.5-1 h ii) water, reflux, 3-4 h, iii) 40% aq. NaOH solution, pH 8; 65-83% yield (b) chloroacetyl chloride, K_2CO_3, DMF, 0-5 ºC to RT, 1-2 h; 78-92% yield (c) Het-SH, K_2CO_3, DMF, RT, 0.5-1 h, 53-92% yield.'

Step 3: Preparation of final compounds STS01-STS25

To a stirred solution of fragments **TDZA01-TDZA05** (1.26 mmol) and suitably substituted thiol compound (Het-SH) (1.26 mmol) in DMF (10 mL) was added pulverized and activated K_2CO_3 (2.52 mmol) at ambient temperature. The resultant suspension was stirred at ambient temperature for 1-2 h. Progress and completion of reaction was monitored by TLC. Upon completion of reaction, the reaction mixture was poured into ice water (100 mL) and vigorously stirred for 15-20 min, followed by filtration of the obtained precipitate under reduced pressure. Alternatively, in case no precipitate was obtained on pouring the reaction mixture into ice water, product was extracted with ethyl acetate (2×50 mL), dried over anhydrous sodium sulphate and solvent evaporated in a rotary evaporator to obtain desired products as powdery solids.

3.2.1.2. Physicochemical characterization

The physicochemical characterizations of all the synthesized compounds of the **STS series** were performed for melting range, solubility, retardation factor (R_f), calculated logP (ClogP), experimental logP (i.e., partitioning in *n*-octanol:water) and appearance of the final compounds (**STS01-STS25**) by identical methodologies as described earlier (**Section 2.2.2.3**).

3.2.1.3. Spectral characterization

The spectral characterization of the intermediates and final compounds (**STS01-STS25**) was done to elucidate their structure and confirm their formation by FTIR, ^{1}H & ^{13}C NMR, MS and HRMS techniques as described in **Section 2.2.2.4**.

3.2.2. Biological studies

3.2.2.1. *In vitro* SHP2 enzyme inhibition assay

The biochemical *in vitro* assay to evaluate SHP2 inhibition activity of the compounds **STS01-STS25** was done by following the fluorescence-based DiFMUP assay using the homogeneous full-length SHP-2 assay kit by allosterically activating fl-SHP2 enzyme prior to substrate addition by incubating with IRS-1 peptide (mentioned in detail in **Section 2.2.3.1**). All experiments were done in duplicate using three different concentrations of the test compounds and results are reported as mean ± SEM.

3.2.2.2. *In vitro* DPPH assay for antioxidant property evaluation

The antioxidant property of some selected compounds of the **STS series** was evaluated by the DPPH assay as described in Chapter 2 (Section **2.2.3.2**).

3.2.2.3. *In vitro* blood-brain barrier permeability assay (PAMPA-BBB) of compound STS23

The *in vitro* blood-barrier permeability of the lead compound of the **STS series** i.e., compound **STS23** was evaluated by the DPPH assay as described in Chapter 2 (Section **2.2.3.3)**.

3.2.2.4. Cell-based assays

3.2.2.4.1. *In vitro* antiproliferation study in cancer cell lines

The *in vitro* anticancer efficacy of those compounds of the **STS series** that displayed submicromolar SHP2 inhibitory activity (IC_{50} < 1.0 μM) was assessed by an MTT assay on MCF-7 cells. Further, the antiproliferation assay of *in vitro* lead compound **STS23** was done in PC12 & U87MG cells by applying method as in **Section 2.2.3.4.2**. All experiments were done in triplicate and results are reported as mean ± SEM.

3.2.2.4.2. Colony formation assay of compound STS09 and STS23

The anti-survival property of compounds **STS09** and **STS23** in MCF-7 cells was determined by conducting a colony formation and scratch wound-healing assay respectively. The protocol for the assay has been described previously in **Section 2.2.3.4.3** and was followed without any modifications.

3.2.2.5. *In vivo* studies

3.2.2.5.1. *In vivo* acute oral toxicity evaluation of compound STS23

All animal experimentations conducted were approved by the Institutional Animals Ethics Committee (IAEC) of Indian Institute of Technology (Banaras Hindu University), Varanasi, India (IAEC Approval Number: IIT(BHU)/IAEC/2024/I/039). The acute oral toxicity of compound **STS23** was determined in adult female Wistar rats in accordance with the OECD Guideline 423 (Acute Toxic Class Method) and the LD_{50} calculated. The method followed for the study and the parameters tested are mentioned in **Section 2.2.3.5.1**.

3.2.3. Computational studies

Post-screening molecular docking of **STS01-STS25** was done in the tunnel allosteric site of SHP2 (PDB ID: 5EHR) to assess their binding affinity and pose analysis in SHP2 allosteric site. This was done in AutoDockTools 4.2 by using the protocol as described earlier in **Section 2.2.4.1** and visualizing the docked conformations in Discovery Studio Visualizer v21.1.0.20298. Further, molecular dynamics simulation study was done for compound **STS23** for 100 ns in the tunnel allosteric site of SHP2 (PDB ID: 5EHR) using Desmond module (described in **Section 2.2.4.2**). Finally, the ADMET properties

of the molecules of the **STS series** were predicted using Pre-ADMET web-based server (as described in **Section 2.2.4.3**).

3.3. Results and discussion

3.3.1. Chemistry

3.3.1.1. Synthesis of final compounds STS01-STS25

The final compounds **STS01-STS25**, were synthesized by the process as shown in **Scheme 3.1**. Initially, the substituted aryl/heteroaryl carboxylic acid was treated with thiosemicarbazide in presence of $POCl_3$ and heated at a temperature of 100ºC for a duration of 0.5-1 h. Thereafter, the reaction mixture was cooled down to ambient temperature and water was added carefully to quench the reaction followed by heating the resultant mixture at a temperature of 100ºC for a duration of 3-4 h to form the fragments **TDZ01-TDZ05**, which were reacted with chloroacetyl chloride in presence of K_2CO_3 in DMF to obtain fragments **TDZA01-TDZA05**. These fragments were then reacted with a suitable thiol compound (Het-SH) in presence of base to afford the final compounds in good yield.

3.3.1.2. Physicochemical characterization of final compounds

All the final compounds of **STS series** (**STS01-STS25**) were obtained in good yield ranging from 67-97 % as powdered solid. Physicochemical characteristics of the final compounds like melting point, ClogP and experimental logP (*n*-octanol/water) were determined and are given in **Table 3.1**. Most of the compounds possessed logP values near the acceptable range for an orally and intestinally bioavailable drug candidate i.e., from 0.65-2.05 with few of the most potent inhibitors exhibiting logP around 2 which is the acceptable value for a CNS-targeting drug molecule.

Table 3.1. Physicochemical characterization data of compounds **STS01**-**STS25**.

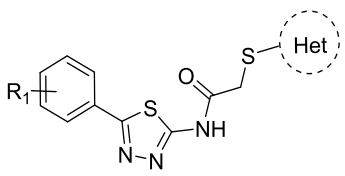

STS01-STS20

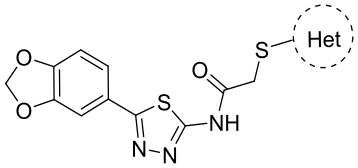

STS21-STS25

Compd Code	R_1	R_2	MW	ClogP[a]	LogP[b]	% yield	Melting range (ºC)	R_f[c]	Appearance
STS01	H	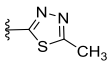	349.44	1.88	1.32	67	212-214	0.72	White solid
STS02	H	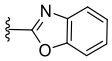	368.43	3.71	1.56	76	223-225	0.75	Off-white solid
STS03	H	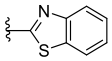	384.49	4.39	0.99	82	203-205	0.64	White solid
STS04	H	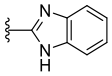	367.44	3.86	1.49	90	185-187	0.52	Off-white solid
STS05	H		333.38	1.67	1.08	95	215-217	0.51	White solid
STS06	4-F	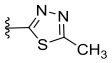	367.44	2.03	1.19	93	204-206	0.85	White solid
STS07	4-F	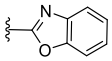	386.42	3.85	2.06	83	200-202	0.80	Brown solid
STS08	4-F	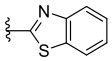	402.48	4.53	1.69	96	199-200	0.58	Off-white solid
STS09	4-F	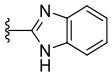	385.43	4.00	2.15	87	220-222	0.63	Light pink solid
STS10	4-F		351.38	1.81	0.96	93	206-208	0.61	Off-white solid
STS11	4-OCH_3	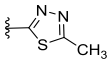	379.47	1.94	1.71	75	218-220	0.68	White solid
STS12	4-OCH_3	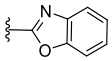	398.55	3.77	1.60	83	206-208	0.66	Dark tan solid
STS13	4-OCH_3	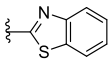	414.46	4.44	0.69	85	202-204	0.53	Tan solid
STS14	4-OCH_3	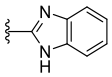	397.47	3.92	2.06	97	184-185	0.62	Light pink solid
STS15	4-OCH_3		363.44	1.73	0.66	90	211-213	0.52	Off-white solid
STS16	3,4-$(OCH_3)_2$	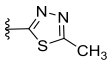	409.49	1.66	1.55	71	205-207	0.75	Off-white solid
STS17	3,4-$(OCH_3)_2$	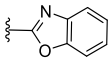	428.48	3.49	0.91	82	228-230	0.72	White solid

STS18	3,4-$(OCH_3)_2$	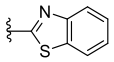	444.54	4.17	1.09	85	208-210	0.65	White solid
STS19	3,4-$(OCH_3)_2$	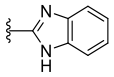	427.49	3.64	1.59	92	246-248	0.68	Light pink solid
STS20	3,4-$(OCH_3)_2$		393.44	1.45	0.58	71	195-197	0.6	Off-white solid
STS21	--	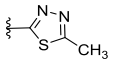	393.45	1.97	0.88	77	214-216	0.56	Light pink solid
STS22	--	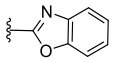	412.44	3.79	0.93	83	223-225	0.84	Off-white solid
STS23	--	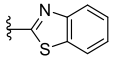	428.50	4.47	0.65	90	196-197	0.67	Off-white solid
STS24	--	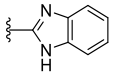	411.49	3.95	1.43	97	207-208	0.59	Light pink solid
STS25	--		377.39	1.75	1.41	89	232-235	0.62	Off-white solid

[a] Calculated using ChemDraw v15.0.0.106. [b] Experimental LogP data. [c] R_f values in 2% MeOH in DCM.

3.3.1.3. Spectral characterization

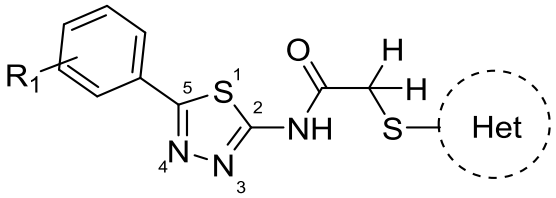

All compounds were characterized by FTIR, ^1H & ^{13}C NMR and HRMS analysis. The analytical data of all synthesized compounds are in good agreement with the predicted and/or calculated data, as applicable. The structure of the final compounds (**STS01-STS25**) was confirmed first by FTIR by obtaining peaks at around ν 3430 cm^{-1} for amide N-H str., around ν 1690 cm^{-1} for amide C=O str., around ν 1570 cm^{-1} for N-H bend. and ν 1340 cm^{-1} for amine C-N str., thereby confirming the thioacetamide structure. The structure was further confirmed by ^1H NMR spectra by the presence of a characteristic singlet peak of two protons between δ 4.0-4.6 ppm which represent the methylene protons (-S-C**H**$_2$-CO-NH-) at the sulfur and acetamide bridge and the amide proton (-CO-N**H**-) appearing as a signal at δ 13 ppm; there were the methylene carbon

(-S-**C**H_2-CO-NH-) around δ 30-40 ppm & the amide carbonyl carbon (-S-CH_2-**C**O-NH-) around δ 166-167 ppm in ^{13}C NMR.

For the homologous clusters according to the R_1 substitution containing the five different heterocycles i.e., TDZT, 1,3,4-thiadiazole-2-thiol (compounds **STS01, STS06, STS11, STS16** and **STS21)**; MBO, 2-mercaptobenzoxazole (compounds **STS02, STS07, STS12, STS17** and **STS22)**; MBT, 2-mercaptobenthiazole (compounds **STS03, STS08, STS13, STS18** and **STS23**); MBI, 2-mercaptobenzimidazole (compounds **STS04, STS09, STS14, STS19** and **STS24**); MMT, 2-methylmercaptotetrazole (compounds **STS05, STS10, STS15, STS20** and **STS25**) (**Table 3.1**), the presence of specific R_1 substitution was confirmed mainly by FTIR and ^{13}C NMR techniques respectively. In FTIR, specific peak was obtained for the 4-fluoro substitution i.e., R_1 = 4-F, at around ν 1230 cm^{-1} (compounds **STS06-STS10**) and for the 4-methoxy (compounds **STS11-STS15**) and 3,4-dimethoxy substitutions (compounds **STS16-STS20**) at around ν 1217 cm^{-1}. In ^{13}C NMR, signal corresponding to the 4-F substitution was obtained at around δ 164 ppm with a prominent -**C**-F, n+1 splitting due to the para position of the fluoro substituent in compounds **STS06-STS10**. Likewise, the 4-OCH_3 substitution was confirmed by a singlet peak at δ 3.83 ppm corresponding to three protons (-C_6H_4-4-OC**H**$_3$) in ^{1}H NMR and a signal at δ 55.88 ppm (-C_6H_4-4-O**C**H_3) in ^{13}C NMR in compounds **STS11-STS15**. The dimethoxy substitution was confirmed similarly by obtaining signal at δ 3.82 ppm corresponding to 6 protons (-C_6H_4-3,4-(OC**H**$_3$)$_2$) with a *J* value of 17.1 Hz; in ^{13}C NMR, it gave two signals at around δ 56 ppm for the two methoxy carbons (C_6H_5-3,4-(O**C**H_3)$_2$) in compounds **STS16-STS20**.

2-((5-Methyl-1,3,4-thiadiazol-2-yl)thio)-*N*-(5-phenyl-1,3,4-thiadiazol-2-yl)acetamide (STS01): White solid; yield = 67%, m.p.: 212-214 ºC; ^{1}H NMR (500 MHz, DMSO-d_6) δ ppm 13.08 (s, 1H, amide -NH), 7.94 (s, 2H), 7.54 (dt, J = 4.5, 2.8 Hz, 3H), 4.44 (s, 2H, -CH_2), 2.68 (s, 3H, -CH_3); ^{13}C NMR (126 MHz, DMSO-d_6) δ ppm 166.82 (-C=O), 166.48, 164.20, 162.60, 158.85, 131.18, 130.54, 129.86, 127.43, 37.08 (-CH_2), 15.67 (-CH_3).

2-(Benzo[*d*]oxazol-2-ylthio)-*N*-(5-phenyl-1,3,4-thiadiazol-2-yl)acetamide (STS02): Off-white solid; yield = 76%, m.p.: 223-225 ºC; FTIR (v, cm^{-1}, KBr) 3430 (amide N-H str.), 1693 (amide C=O str.), 1573 (N-H bend.), 1343 (amine C-N str.); ^{1}H NMR (500 MHz, DMSO-d_6) δ ppm 13.17 (s, 1H, amide -NH), 8.00 – 7.91 (m, 2H), 7.73 – 7.60 (m, 2H), 7.57 – 7.50 (m, 3H), 7.39 – 7.29 (m, 2H), 4.54 (s, 2H, -CH_2); ^{13}C NMR (126 MHz, DMSO-d_6) δ ppm 166.56 (-C=O), 163.86, 158.83, 151.88, 141.59, 131.19, 130.50, 129.85, 127.43, 125.21, 124.94, 118.82, 110.77, 35.88 (-CH_2); MS (ESI$^-$): calculated for $C_{17}H_{12}N_4O_2S_2$ [M-H]$^-$, 367.04; found, 366.95; HRMS: calcd for $C_{17}H_{12}N_4O_2S_2$ [M+H]$^+$ 369.0480, found 369.0481.

2-(Benzo[*d*]thiazol-2-ylthio)-*N*-(5-phenyl-1,3,4-thiadiazol-2-yl)acetamide (STS03): White solid; yield = 82%, m.p.: 203-205 ºC; FTIR (v, cm^{-1}, KBr) 3431 (amide N-H str.), 1700 (amide C=O str.), 1564 (N-H bend.), 1330 (amine C-N str.), 1005 (C-S str.); ^{1}H NMR (500 MHz, DMSO-d_6) δ ppm 13.14 (s, 1H, amide -NH), 8.04 (d, J = 8.1 Hz, 1H), 7.97 – 7.91 (m, 2H), 7.81 (d, J = 7.9 Hz, 1H), 7.53 (d, J = 6.7 Hz, 3H), 7.49 – 7.43 (m, 1H), 7.38 (t, J = 7.0 Hz, 1H), 4.56 (s, 2H, -CH_2); ^{13}C NMR (126 MHz, DMSO-d_6) δ ppm 166.82 (-C=O), 165.89, 162.66, 152.87, 135.33, 131.16, 130.43, 129.87, 127.43, 126.95, 125.14, 122.45, 121.64, 36.72 (-CH_2); HRMS: calcd for $C_{17}H_{12}N_4OS_3$ [M+H]$^+$ 385.0251, found 385.0255.

2-((1*H*-Benzo[*d*]imidazol-2-yl)thio)-*N*-(5-phenyl-1,3,4-thiadiazol-2-yl)acetamide (STS04): Off-white solid; yield = 90%, m.p.: 185-187 ºC; FTIR (*v*, cm^{-1}, KBr) 3197 (amide N-H str.), 1621 (amide C=O str.), 1577 (N-H bend.), 1270 (amine C-N str.); ^{1}H NMR (500 MHz, DMSO-d_6) δ ppm 7.86 (d, *J* = 7.8 Hz, 2H), 7.56 – 7.33 (m, 5H), 7.12 (dd, *J* = 6.0, 3.3 Hz, 2H), 4.12 (s, 2H, -CH_2); ^{13}C NMR (126 MHz, DMSO-d_6) δ ppm 172.21, 168.22 (-C=O), 158.92, 151.97, 140.07, 132.88, 129.51, 126.67, 121.67, 114.29, 38.94 (-CH_2); MS (ESI^-): calculated for $C_{17}H_{13}N_5OS_2$ $[M-H]^-$, 366.06; found, 366.00; HRMS: calcd for $C_{17}H_{13}N_5OS_2$ $[M+H]^+$ 368.0640, found 368.0638.

2-((1-Methyl-1*H*-tetrazol-5-yl)thio)-*N*-(5-phenyl-1,3,4-thiadiazol-2-yl)acetamide (STS05): White solid; yield = 95%, m.p.: 215-217 ºC; FTIR (*v*, cm^{-1}, KBr) 3410 (amide N-H str.), 1697 (amide C=O str.), 1551 (N-H bend.), 1333 (amine C-N str.); ^{1}H NMR (500 MHz, DMSO-d_6) δ ppm 7.82 (dd, *J* = 8.4, 1.4 Hz, 2H), 7.47 – 7.42 (m, 2H), 7.40 – 7.34 (m, 1H), 4.11 (s, 2H, -CH_2), 3.99 (s, 3H, -NCH_3); ^{13}C NMR (126 MHz, DMSO-d_6) δ ppm 170.71, 169.61 (-C=O), 158.07, 155.01, 133.37, 129.41, 129.10, 126.51, 41.40 (-CH_2), 34.00 (-NCH_3); MS (ESI^-): calculated for $C_{12}H_{11}N_7OS_2$ $[M-H]^-$, 332.04; found, 331.95; HRMS: calcd for $C_{12}H_{11}N_7OS_2$ $[M+H]^+$ 334.0544, found 334.0542.

***N*-(5-(4-Fluorophenyl)-1,3,4-thiadiazol-2-yl)-2-((5-methyl-1,3,4-thiadiazol-2-yl)thio)acetamide (STS06):** White solid; yield = 93%, m.p.: 204-206 ºC; FTIR (*v*, cm^{-1}, KBr) 3404 (amide N-H str.), 1677 (amide C=O str.), 1545 (N-H bend.), 1242 (C-F str.); ^{1}H NMR (500 MHz, DMSO-d_6) δ ppm 7.92 – 7.82 (m, 2H), 7.35 – 7.24 (m, 2H), 4.13 (s, 2H, -CH_2), 2.66 (s, 3H, -CH_3); ^{13}C NMR (126 MHz, DMSO-d_6) δ ppm 170.68, 168.63 (-C=O), 166.91, 165.32, 163.82 (-C-F, n+1 splitting), 161.86 (-C-F, n+1 splitting), 157.51, 129.69, 129.66, 128.66, 128.60, 116.54, 116.37, 41.72 (-CH_2), 15.62 (-CH_3); MS (ESI^-): calculated for $C_{13}H_{10}FN_5OS_3$ $[M-H]^-$, 366.00; found, 366.00

(100%), 366.95 (50%), 367.95 (25%); HRMS: calcd for $C_{13}H_{10}FN_5OS_3$ $[M+H]^+$ 368.0110, found 368.0114.

2-(Benzo[*d*]oxazol-2-ylthio)-*N*-(5-(4-fluorophenyl)-1,3,4-thiadiazol-2-yl)acetamide (STS07): Brown solid; yield = 83%, m.p.: 200-202 ºC; FTIR (ν, cm^{-1}, KBr) 3403 (amide N-H str.), 1673 (amide C=O str.), 1544 (N-H bend.), 1322 (amine C-N str.), 1234 (C-F str.); ^{1}H NMR (500 MHz, DMSO-d_6) δ ppm 7.91 (dd, J = 8.9, 5.5 Hz, 2H), 7.68 – 7.57 (m, 2H), 7.31 (ddd, J = 8.9, 5.1, 2.8 Hz, 4H), 4.33 (s, 2H, -CH_3); ^{13}C NMR (126 MHz, DMSO-d_6) δ ppm 169.59 (-C=O), 165.37, 164.02 (Ar, -C-F), 162.06, 158.33, 151.69, 141.90, 129.19, 128.90, 128.83, 124.98, 124.54, 118.61, 116.62, 116.45, 110.58, 39.04 (-CH_2); MS (ESI^-): calculated for $C_{17}H_{11}FN_4O_2S_2$ $[M-H]^-$, 385.03; found, 385.00 (100%), 386.00 (25%), 387.00 (12.5%); HRMS: calcd for $C_{17}H_{11}FN_4O_2S_2$ $[M+H]^+$ 387.0385, found 387.0391.

2-(Benzo[*d*]thiazol-2-ylthio)-*N*-(5-(4-fluorophenyl)-1,3,4-thiadiazol-2-yl)acetamide (STS08): Off-white solid; yield = 96%, m.p.: 199-200 ºC; FTIR (ν, cm^{-1}, KBr) 3361 (amide N-H str.), 1692 (amide C=O str.), 1565 (N-H bend.), 1300 (amine C-N str.), 1235 (C-F str.), 992 (C-S str.); ^{1}H NMR (500 MHz, DMSO-d_6) δ ppm 13.19 (s, 1H, amide -NH), 8.09 – 7.92 (m, 3H), 7.80 (d, J = 7.9 Hz, 1H), 7.48 – 7.41 (m, 1H), 7.41 – 7.29 (m, 3H), 4.55 (s, 2H, -CH_3); ^{13}C NMR (126 MHz, DMSO-d_6) δ ppm 167.20 (-C=O), 166.12, 166.08 (-C-F, n+1 splitting), 164.74 (-C-F, n+1 splitting), 161.20, 159.69 (-S-C(=N-)NH, n+1 splitting), 159.57 (-S-C(=N-)NH, n+1 splitting), 152.91, 135.31, 129.72, 129.65, 127.38, 127.36, 126.91, 125.08, 122.41, 121.61, 116.97, 116.79, 37.08 (-CH_2); MS (ESI^-): calculated for $C_{17}H_{11}FN_4OS_3$ $[M-H]^-$, 401.00; found, 401.00 (100%), 402.00 (25%), 402.95 (12.5%); HRMS: calcd for $C_{17}H_{11}FN_4OS_3$ $[M+H]^+$ 403.0157, found 403.0173.

2-((1*H*-Benzo[*d*]imidazol-2-yl)thio)-*N*-(5-(4-fluorophenyl)-1,3,4-thiadiazol-2-yl)acetamide (STS09): Light pink solid; yield = 87%, m.p.: 220-222 ºC; FTIR (*v*, cm^{-1}, KBr) 3424 (amide N-H str.), 1691 (amide C=O str.), 1563 (N-H bend.), 1331 (amine C-N str.), 1267 (C-F str.); ^{1}H NMR (500 MHz, DMSO-d_6) δ ppm 12.82 (s, 1H, amide -NH), 7.92 – 7.86 (m, 2H), 7.46 (dd, *J* = 6.0, 3.2 Hz, 2H), 7.30 (t, *J* = 8.9 Hz, 2H), 7.11 (dd, *J* = 6.0, 3.2 Hz, 2H), 4.08 (s, 2H, $-CH_2$); ^{13}C NMR (126 MHz, DMSO-d_6) δ ppm 172.52, 168.89 (-C=O), 163.82, 162.84, 161.86, 157.56, 152.11, 140.06, 129.73, 129.70, 128.66, 128.59, 121.63, 116.55, 116.38, 114.26, 39.18 ($-CH_2$); MS (ESI^-): calculated for $C_{17}H_{12}FN_5OS_2$ $[M-H]^-$, 384.05; found, 384.00 (100%), 385.00 (33.34%), 386.00 (16.67%); HRMS: calcd for $C_{17}H_{12}FN_5OS_2$ $[M+H]^+$ 386.0545, found 386.0557.

***N*-(5-(4-Fluorophenyl)-1,3,4-thiadiazol-2-yl)-2-((1-methyl-1*H*-tetrazol-5-yl)thio)acetamide (STS10):** Off-white solid; yield = 93%, m.p.: 206-208 ºC; FTIR (*v*, cm^{-1}, KBr) 3198 (amide N-H str.), 1516 (N-H bend.), 1335 (amine C-N str.), 1238 (C-F str.); ^{1}H NMR (500 MHz, DMSO-d_6) δ ppm 7.86 (dd, *J* = 8.9, 5.5 Hz, 2H), 7.29 (t, *J* = 8.9 Hz, 2H), 4.13 (s, 2H, $-CH_2$), 3.99 (s, 3H, $-NCH_3$); ^{13}C NMR (126 MHz, DMSO-d_6) δ ppm 170.77, 169.59 (-C=O), 163.74, 161.79, 157.21, 154.94, 129.86, 129.83, 128.58, 128.52, 116.51, 116.33, 41.24 ($-CH_2$), 34.02 ($-NCH_3$); MS (ESI^-): calculated for $C_{12}H_{10}FN_7OS_2$ $[M-H]^-$, 350.04; found, 350.00 (100%), 351.00 (41.67%), 352.00 (20.84%); HRMS: calcd for $C_{12}H_{10}FN_7OS_2$ $[M+H]^+$ 352.0450, found 352.0454.

***N*-(5-(4-Methoxyphenyl)-1,3,4-thiadiazol-2-yl)-2-((5-methyl-1,3,4-thiadiazol-2-yl)thio)acetamide (STS11):** White solid; yield = 75%, m.p.: 218-220 ºC; FTIR (*v*, cm^{-1}, KBr) 3384 (amide N-H str.), 1699 (amide C=O str.), 1378 (amine C-N str.), 1237 (alkyl ether C-O str.); ^{1}H NMR (500 MHz, DMSO-d_6) δ ppm 12.99 (s, 1H, amide -NH), 7.88 (d, *J* = 8.7 Hz, 2H), 7.08 (d, *J* = 9.0 Hz, 2H), 4.42 (s, 2H, $-CH_2$), 3.83 (s, 3H, -

OCH_3), 2.68 (s, 3H, -CH_3); ^{13}C NMR (126 MHz, DMSO-d_6) δ ppm 166.70 (-C=O), 166.46, 164.24, 162.39, 161.60, 158.23, 129.00, 123.07, 115.24, 55.89 (-OCH_3), 37.11 (-CH_2), 15.67 (-CH_3); MS (ESI$^-$): calculated for $C_{14}H_{13}N_5O_2S_3$ [M-H]$^-$, 378.02; found, 377.95; HRMS: calcd for $C_{14}H_{13}N_5O_2S_3$ [M+H]$^+$ 380.0309, found 380.0307.

2-(Benzo[*d*]oxazol-2-ylthio)-*N*-(5-(4-methoxyphenyl)-1,3,4-thiadiazol-2-yl)acetamide (STS12): Dark tan solid; yield = 83%, m.p.: 206-208 ºC; FTIR (ν, cm^{-1}, KBr) 3426 (amide N-H str.), 1696 (amide C=O str.), 1580 (N-H bend.), 1336 (amine C-N str.), 1253 (alkyl ether C-O str.); ^{1}H NMR (500 MHz, DMSO-d_6) δ ppm 13.05 (s, 1H, amide -NH), 7.85 (d, J = 8.9 Hz, 2H), 7.77 – 7.55 (m, 2H), 7.42 – 7.24 (m, 2H), 7.06 (d, J = 8.9 Hz, 2H), 4.48 (s, 2H, -CH_2), 3.82 (s, 3H, -OCH_3); ^{13}C NMR (126 MHz, DMSO-d_6) δ ppm 167.06, 164.21 (-C=O), 161.76, 161.39, 151.83, 141.66, 128.83, 125.16, 124.85, 123.51, 118.77, 115.17, 110.73, 55.86 (-OCH_3), 36.57 (-CH_2); MS (ESI$^-$): calculated for $C_{18}H_{14}N_4O_3S_2$ [M-H]$^-$, 397.05; found, 397.00; HRMS: calcd for $C_{18}H_{14}N_4O_3S_2$ [M+H]$^+$ 399.0585, found 399.0582.

2-(Benzo[*d*]thiazol-2-ylthio)-*N*-(5-(4-methoxyphenyl)-1,3,4-thiadiazol-2-yl)acetamide (STS13): Tan solid; yield = 85%, m.p.: 202-204 ºC; FTIR (ν, cm^{-1}, KBr) 3425 (amide N-H str.), 1685 (amide C=O str.), 1580 (N-H bend.), 1340 (amine C-N str.), 1258 (alkyl ether C-O str.); ^{1}H NMR (500 MHz, DMSO-d_6) δ ppm 13.07 (s, 1H, amide -NH), 8.03 (d, J = 7.9 Hz, 1H), 7.87 (d, J = 8.9 Hz, 2H), 7.80 (d, J = 8.2 Hz, 1H), 7.46 (t, J = 7.7 Hz, 1H), 7.37 (t, J = 7.6 Hz, 1H), 7.07 (d, J = 8.9 Hz, 2H), 4.54 (s, 2H, -CH_2), 3.82 (s, 3H, -OCH_3); ^{13}C NMR (126 MHz, DMSO-d_6) δ ppm 166.75 (-C=O), 165.95, 162.78, 161.58, 158.32, 152.88, 135.32, 128.98, 126.93, 125.12, 123.08, 122.43, 121.63, 115.23, 55.88 (-OCH_3), 36.81 (-CH_2); MS (ESI$^-$): calculated for

$C_{18}H_{14}N_4O_2S_3$ [M-H]$^-$, 413.02; found, 412.95; HRMS: calcd for $C_{18}H_{14}N_4O_2S_3$ [M+H]$^+$ 415.0357, found 415.0364.

2-((1*H*-Benzo[d]imidazol-2-yl)thio)-*N*-(5-(4-methoxyphenyl)-1,3,4-thiadiazol-2-yl)acetamide (**STS14**): Light pink solid; yield = 97%, m.p.: 184-185 ºC; FTIR (*v*, cm^{-1}, KBr) 3425 (amide N-H str.), 1698 (amide C=O str.), 1577 (N-H bend.), 1364 (amine C-N str.), 1253 (alkyl ether C-O str.); ^{1}H NMR (500 MHz, DMSO-d_6) δ ppm 7.78 (d, *J* = 8.9 Hz, 2H), 7.45 (dd, *J* = 6.0, 3.2 Hz, 2H), 7.11 (dd, *J* = 6.0, 3.1 Hz, 2H), 7.02 (d, *J* = 8.9 Hz, 2H), 4.03 (s, 2H, -CH_2), 3.80 (s, 3H, -OCH_3); ^{13}C NMR (126 MHz, DMSO-d_6) δ ppm 172.12 (-C=O), 160.34, 158.65, 152.22, 128.04, 125.71, 121.60, 114.88, 114.27, 55.73 (-OCH_3), 39.03 (-CH_2); MS (ESI$^-$): calculated for $C_{18}H_{15}N_5O_2S_2$ [M-H]$^-$, 396.06; found, 396.00; HRMS: calcd for $C_{18}H_{15}N_5O_2S_2$ [M+H]$^+$ 398.0745, found 398.0741.

***N*-(5-(4-Methoxyphenyl)-1,3,4-thiadiazol-2-yl)-2-((1-methyl-1*H*-tetrazol-5-yl)thio)acetamide** (**STS15**): Off-white solid; yield = 90%, m.p.: 211-213 ºC; FTIR (*v*, cm^{-1}, KBr) 3219 (amide N-H str.), 1657 (amide C=O str.), 1578 (N-H bend.), 1253 (alkyl ether C-O str.); ^{1}H NMR (500 MHz, DMSO-d_6) δ ppm 7.75 (d, *J* = 8.9 Hz, 2H), 7.01 (d, *J* = 8.9 Hz, 2H), 4.10 (s, 2H, -CH_2), 3.99 (s, 3H, -NCH_3), 3.80 (s, 3H, -OCH_3); ^{13}C NMR (126 MHz, DMSO-d_6) δ ppm 170.42, 169.02 (-C=O), 160.14, 158.03, 155.05, 127.90, 126.06, 114.81, 55.70, 41.42 (-CH_2), 33.99 (-NCH_3); MS (ESI$^-$): calculated for $C_{13}H_{13}N_7O_2S_2$ [M-H]$^-$, 362.05; found, 362.00; HRMS: calcd for $C_{13}H_{13}N_7O_2S_2$ [M+H]$^+$ 364.0650, found 364.0647.

***N*-(5-(3,4-Dimethoxyphenyl)-1,3,4-thiadiazol-2-yl)-2-((5-methyl-1,3,4-thiadiazol-2-yl)thio)acetamide (STS16):** Off=white solid; yield = 71%, m.p.: 205-207 ºC; FTIR

(*v*, cm^{-1}, KBr) 3373 (amide N-H str.), 1664 (amide C=O str.), 1577 (N-H bend.), 1376 (amine C-N str.), 1250 (alkyl ether C-O str.); ^{1}H NMR (500 MHz, DMSO-d_6) δ ppm 7.46 (s, 1H), 7.33 (d, J = 6.3 Hz, 1H), 7.04 (d, J = 8.4 Hz, 1H), 4.17 (s, 2H, $-CH_2$), 3.82 (d, J = 17.1 Hz, 6H, 2x($-OCH_3$)), 2.67 (s, 3H, $-CH_3$); ^{13}C NMR (126 MHz, DMSO-d_6) δ ppm 169.68, 169.39, 166.49 (-C=O), 165.47, 150.27, 149.41, 125.39, 119.96, 112.42, 109.34, 56.07 ($-OCH_3$), 55.94 ($-OCH_3$), 40.93 ($-CH_2$), 15.63 ($-CH_3$); MS (ESI^-): calculated for $C_{15}H_{15}N_5O_3S_3$ $[M-H]^-$, 408.03; found, 408.00; HRMS: calcd for $C_{15}H_{15}N_5O_3S_3$ $[M+H]^+$ 410.0415, found 410.0408.

2-(Benzo[*d*]oxazol-2-ylthio)-*N*-(5-(3,4-dimethoxyphenyl)-1,3,4-thiadiazol-2-yl)acetamide (STS17): White solid; yield = 82%, m.p.: 228-230 ºC; FTIR (*v*, cm^{-1}, KBr) 3405 (amide N-H str.), 1651 (amide C=O str.), 1530 (N-H bend.), 1391 (amine C-N str.), 1247 (alkyl ether C-O str.); ^{1}H NMR (500 MHz, DMSO-d_6) δ ppm 13.10 (s, 1H), 7.69 – 7.60 (m, 2H), 7.49 (d, J = 2.1 Hz, 1H), 7.43 (dd, J = 8.3, 2.1 Hz, 1H), 7.36 – 7.30 (m, 2H), 7.07 (d, J = 8.4 Hz, 1H), 4.49 (s, 2H, $-CH_2$), 3.83 (d, J = 14.4 Hz, 6H, 2x($-OCH_3$)); ^{13}C NMR (126 MHz, DMSO-d_6) δ ppm 166.87 (-C=O), 164.09, 162.17, 159.39, 151.83, 151.22, 149.55, 141.64, 125.18, 124.88, 123.40, 120.76, 118.79, 112.46, 110.74, 109.72, 56.11 ($-OCH_3$), 56.03 ($-OCH_3$), 36.33 ($-CH_2$); MS (ESI^-): calculated for $C_{19}H_{16}N_4O_4S_2$ $[M-H]^-$, 427.06; found, 427.00; HRMS: calcd for $C_{19}H_{16}N_4O_4S_2$ $[M+H]^+$ 429.0691, found 429.0708.

2-(Benzo[*d*]thiazol-2-ylthio)-*N*-(5-(3,4-dimethoxyphenyl)-1,3,4-thiadiazol-2-yl)acetamide (STS18): White solid; yield = 85%, m.p.: 208-210 ºC; FTIR (*v*, cm^{-1}, KBr) 3340 (amide N-H str.), 1678 (amide C=O str.), 1516 (N-H bend.), 1396 (amine C-N str.), 1271 (alkyl ether C-O str.); ^{1}H NMR (500 MHz, DMSO-d_6) δ ppm 12.96 (s, 1H, amide -NH), 8.03 (dd, J = 7.9, 1.2 Hz, 1H), 7.85 – 7.77 (m, 1H), 7.53 – 7.41 (m,

3H), 7.37 (ddd, *J* = 8.2, 7.2, 1.2 Hz, 1H), 7.07 (d, *J* = 8.4 Hz, 1H), 4.52 (s, 2H, -CH_2), 3.83 (d, *J* = 14.7 Hz, 6H, 2x(-OCH_3)); ^{13}C NMR (126 MHz, DMSO-d_6) δ ppm 166.96, 166.09 (-C=O), 162.33, 158.96, 152.91, 151.27, 149.56, 135.31, 126.92, 125.09, 123.29, 122.40, 121.61, 120.80, 112.46, 109.75, 56.11 (-OCH_3), 56.04 (-OCH_3), 37.05 (-CH_2); MS (ESI$^-$): calculated for $C_{19}H_{16}N_4O_3S_3$ $[M-H]^-$, 443.03; found, 442.95; HRMS: calcd for $C_{19}H_{16}N_4O_3S_3$ $[M+H]^+$ 445.0463, found 445.0460.

2-((1*H*-Benzo[*d*]imidazol-2-yl)thio)-*N*-(5-(3,4-dimethoxyphenyl)-1,3,4-thiadiazol-2-yl)acetamide (STS19): Light pink solid; yield = 92%, m.p.: 246-248 ºC; FTIR (*v*, cm^{-1}, KBr) 3388 (amide N-H str.), 1701 (amide C=O str.), 1580 (N-H bend.), 1395 (amine C-N str.), 1273 (alkyl ether C-O str.); ^{1}H NMR (500 MHz, DMSO-d_6) δ ppm 7.50 – 7.41 (m, 3H), 7.32 (d, *J* = 8.2 Hz, 1H), 7.11 (dd, *J* = 6.0, 3.2 Hz, 2H), 7.03 (d, *J* = 8.4 Hz, 1H), 4.04 (s, 2H, -CH_2), 3.84 (s, 3H, -OCH_3), 3.80 (s, 3H, -OCH_3); ^{13}C NMR (126 MHz, DMSO-d_6) δ ppm 172.16 (-C=O), 158.79, 152.18, 150.07, 149.38, 125.83, 121.60, 119.80, 114.27, 112.40, 109.24, 56.05 (-OCH_3), 55.91 (-OCH_3), 39.07 (-CH_2); MS (ESI$^-$): calculated for $C_{19}H_{17}N_5O_3S_2$ $[M-H]^-$, 426.03; found, 426.00; HRMS: calcd for $C_{19}H_{17}N_5O_3S_2$ $[M+H]^+$ 428.0851, found 428.0844.

***N*-(5-(3,4-Dimethoxyphenyl)-1,3,4-thiadiazol-2-yl)-2-((1-methyl-1*H*-tetrazol-5-yl)thio)acetamide (STS20):** Off-white solid; yield = 71%, m.p.: 195-197 ºC; FTIR (*v*, cm^{-1}, KBr) 3570 (amide N-H str.), 1581 (N-H bend.), 1272 (alkyl ether C-O str.); ^{1}H NMR (500 MHz, DMSO-d_6) δ ppm 7.46 (d, *J* = 2.0 Hz, 1H), 7.30 (dd, *J* = 8.3, 2.1 Hz, 1H), 7.02 (d, *J* = 8.4 Hz, 1H), 4.12 (s, 2H, -CH_2), 3.99 (s, 3H, -NCH_3), 3.83 (s, 3H, -OCH_3), 3.80 (s, 3H, -OCH_3); ^{13}C NMR (126 MHz, DMSO-d_6) δ ppm 170.24, 168.54 (-C=O), 158.43, 154.96, 149.96, 149.36, 126.02, 119.72, 112.36, 109.18, 56.04 (-OCH_3), 55.90 (-OCH_3), 41.15 (-CH_2), 34.01 (-NCH_3); MS (ESI$^-$): calculated for $C_{14}H_{15}N_7O_3S_2$

$[M-H]^-$, 392.06; found, 392.00; HRMS: calcd for $C_{14}H_{15}N_7O_3S_2$ $[M+H]^+$ 394.0756, found 394.0756.

***N*-(5-(Benzo[*d*][1,3]dioxol-5-yl)-1,3,4-thiadiazol-2-yl)-2-((5-methyl-1,3,4-thiadiazol-2-yl)thio)acetamide (STS21):** Light pink solid; yield = 77%, m.p.: 214-216 ºC; FTIR (*v*, cm^{-1}, KBr) 3418 (amide N-H str.), 1653 (amide C=O str.), 1595 (N-H bend.), 1272 (alkyl ether C-O str.); ^{1}H NMR (500 MHz, DMSO-d_6) δ ppm 7.39 (d, J = 1.7 Hz, 1H), 7.27 (dd, J = 8.1, 1.7 Hz, 1H), 6.98 (d, J = 8.1 Hz, 1H), 6.08 (s, 2H, -O-CH_2-O-), 4.09 (s, 2H, -CH_2), 2.67 (s, 3H, -CH_3); ^{13}C NMR (126 MHz, DMSO-d_6) δ ppm 170.49, 167.08 (-C=O), 165.18, 158.12, 148.30, 148.27, 127.52, 121.07, 109.16, 106.18, 101.81 (-O-CH_2-O-), 41.97 (-CH_2), 15.61 (-CH_3); HRMS: calcd for $C_{14}H_{11}N_5O_3S_3$ $[M+H]^+$ 394.0102, found 394.0117.

***N*-(5-(Benzo[*d*][1,3]dioxol-5-yl)-1,3,4-thiadiazol-2-yl)-2-(benzo[*d*]oxazol-2-ylthio)acetamide (STS22):** Off-white solid; yield = 83%, m.p.: 223-225 ºC; FTIR (*v*, cm^{-1}, KBr) 3386 (amide N-H str.), 1665 (amide C=O str.), 1568 (N-H bend.), 1370 (amine C-N str.), 1263 (alkyl ether C-O str.); ^{1}H NMR (500 MHz, DMSO-d_6) δ ppm 13.14 (s, 1H, amide -NH), 7.67 – 7.61 (m, 2H), 7.46 (d, J = 1.8 Hz, 1H), 7.38 (dd, J = 8.1, 1.8 Hz, 1H), 7.35 – 7.31 (m, 2H), 7.03 (d, J = 8.1 Hz, 1H), 6.11 (s, 2H, -O-CH_2-O-), 4.43 (s, 2H, -CH_2); ^{13}C NMR (126 MHz, DMSO-d_6) δ ppm 167.76 (-C=O), 164.54, 162.23, 159.39, 151.80, 150.26, 148.49, 141.94, 125.11, 124.77, 123.10, 122.02, 118.74, 110.70, 109.36, 109.14, 102.13 (-O-CH_2-O-), 38.91 (-CH_2); HRMS**:** calcd for $C_{18}H_{12}N_4O_4S_2$ $[M+H]^+$ 413.0378, found 413.0380.

***N*-(5-(Benzo[*d*][1,3]dioxol-5-yl)-1,3,4-thiadiazol-2-yl)-2-(benzo[*d*]thiazol-2-ylthio)acetamide (STS23):** Off-white solid; yield = 90%, m.p.: 196-197 ºC; FTIR (*v*,

cm^{-1}, KBr) 3383 (amide N-H str.), 1681 (amide C=O str.), 1576 (N-H bend.), 1341 (amine C-N str.), 1287 (alkyl ether C-O str.); ^{1}H NMR (500 MHz, DMSO-d_6) δ ppm 13.14 (s, 1H, amide -NH), 8.03 (dd, J = 8.1, 1.5 Hz, 1H), 7.81 (dd, J = 8.2, 1.4 Hz, 1H), 7.48 – 7.44 (m, 2H), 7.40 – 7.36 (m, 2H), 7.03 (d, J = 8.1 Hz, 1H), 6.12 (s, 2H, -O-CH_2-O-), 4.49 (s, 2H, -CH_2); ^{13}C NMR (126 MHz, DMSO-d_6) δ ppm 166.44 (-C=O), 163.22, 161.49, 160.06, 152.99, 149.53, 148.53, 135.28, 126.89, 125.01, 122.37, 122.18, 121.59, 109.40, 106.80, 102.19 (-O-CH_2-O-), 40.60 (-CH_2); HRMS: calcd for $C_{18}H_{12}N_4O_3S_3$ $[M+H]^+$ 429.0150, found 429.0160.

2-((1*H*-Benzo[d]imidazol-2-yl)thio)-*N*-(5-(benzo[d][1,3]dioxol-5-yl)-1,3,4-thiadiazol-2-yl)acetamide (STS24): Light pink solid; yield = 97%, m.p.: 207-208 ºC; FTIR (v, cm^{-1}, KBr) 3376 (amide N-H str.), 1695 (amide C=O str.), 1573 (N-H bend.), 1355 (amine C-N str.), 1260 (alkyl ether C-O str.); ^{1}H NMR (500 MHz, DMSO-d_6) δ ppm 12.53 (s, 1H, amide -NH), 7.45 (dd, J = 5.9, 3.1 Hz, 2H), 7.41 (d, J = 1.8 Hz, 1H), 7.30 (dd, J = 8.1, 1.8 Hz, 1H), 7.11 (dd, J = 6.0, 3.2 Hz, 2H), 6.99 (d, J = 8.1 Hz, 1H), 6.08 (s, 2H, -O-CH_2-O-), 4.05 (s, 2H, -CH_2); ^{13}C NMR (126 MHz, DMSO-d_6) δ ppm 171.97, 164.50, 158.64, 152.07, 148.47, 148.31, 139.68, 136.63, 127.22, 121.60, 121.22, 114.27, 109.20, 106.27, 101.86 (-O-CH_2-O-), 38.87 (-CH_2); HRMS: calcd for $C_{18}H_{13}N_5O_3S_2$ $[M+H]^+$ 412.0538, found 412.0533.

***N*-(5-(Benzo[*d*][1,3]dioxol-5-yl)-1,3,4-thiadiazol-2-yl)-2-((1-methyl-1*H*-tetrazol-5-yl)thio)acetamide (STS25):** Off-white solid; yield = 89%, m.p.: 232-235 ºC; FTIR (v, cm^{-1}, KBr) 3419 (amide N-H str.), 1588 (N-H bend.), 1336 (amine C-N str.), 1258 (alkyl ether C-O str.); ^{1}H NMR (500 MHz, DMSO-d_6) δ ppm 7.39 (d, J = 1.7 Hz, 1H), 7.27 (d, J = 9.9 Hz, 1H), 6.98 (d, J = 8.1 Hz, 1H), 6.08 (s, 2H, -O-CH_2-O-), 4.10 (s, 2H, -CH_2), 3.99 (s, 3H, -NCH_3); ^{13}C NMR (126 MHz, DMSO-d_6) δ ppm 170.35, 167.39 (-

C=O), 157.72, 154.67, 148.26, 140.70, 127.30, 121.05, 109.14, 106.17, 101.79 (-O-CH_2-O-), 41.15 (-CH_2), 34.00 (-NCH_3); HRMS: calcd for $C_{13}H_{11}N_7O_3S_2$ $[M+H]^+$ 378.0443, found 378.0452.

3.3.2. Biological studies

3.3.2.1. *In vitro* SHP2 inhibition assay

The SHP2 inhibitory activity of final compounds **STS01-STS25** was determined using BPS Bioscience Kit No.: 72330 in allosterically activated full-length his-tag SHP2 enzyme by following the fluorescence-based protocol using DiFMUP as the fluorogenic substrate. The SHP2 IC_{50} values of all the compounds are given in **Table 3.2** along with that of the reference inhibitor **SHP099** (reported data) [94]. All final compounds of the **STS series** showed SHP2 inhibition in micromolar to submicromolar range; IC_{50} values range from 0.321 ± 0.004 µM for compound **STS23** to 1.421 ± 0.085 µM for compound **STS12.** Thus, compound **STS23** emerged as the lead compound as per the SHP2 inhibitory potency.

Table 3.2. *In vitro* enzyme inhibition results of compounds **STS01-STS25**

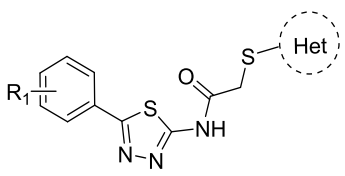

STS01-STS20

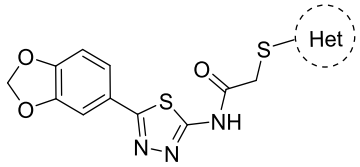

STS21-STS25

Compd Code	R_1	Het	SHP2 IC_{50} (μM)[a]	Compd Code	R_1	Het	SHP2 IC_{50} (μM)[a]
STS01	H	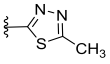	1.100 ± 0.005	**STS14**	4-OCH_3	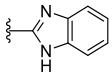	0.914 ± 0.001
STS02	H	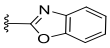	1.130 ± 0.012	**STS15**	4-OCH_3		1.233 ± 0.168
STS03	H	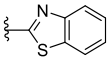	0.956 ± 0.012	**STS16**	3,4-di-OCH_3	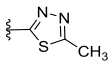	0.780 ± 0.008
STS04	H	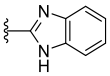	0.915 ± 0.011	**STS17**	3,4-di-OCH_3	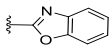	1.045 ± 0.012
STS05	H		1.016 ± 0.081	**STS18**	3,4-di-OCH_3	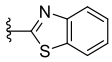	0.737 ± 0.008
STS06	4-F	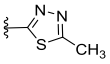	0.844 ± 0.001	**STS19**	3,4-di-OCH_3	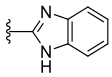	1.024 ± 0.005
STS07	4-F	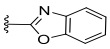	0.784 ± 0.051	**STS20**	3,4-di-OCH_3		0.969 ± 0.049
STS08	4-F	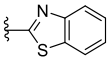	0.540 ± 0.023	**STS21**	--	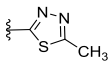	0.908 ± 0.011
STS09	4-F	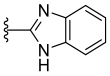	0.859 ± 0.023	**STS22**	--	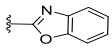	0.781 ± 0.020
STS10	4-F		1.084 ± 0.019	**STS23**	--	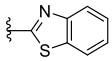	0.321 ± 0.004
STS11	4-OCH_3	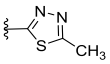	0.842 ± 0.015	**STS24**	--	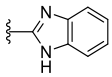	1.130 ± 0.006
STS12	4-OCH_3	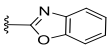	1.421 ± 0.085	**STS25**	--		0.982 ± 0.016
STS13	4-OCH_3	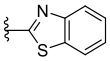	0.880 ± 0.083	**SHP099**	--	--	0.070[b]

[a] Values represent the assay drug concentration that give 50% inhibition of SHP2 activity and are the mean ± SEM of two independent experiments done in duplicate; statistical significance: $p<0.05$ versus the corresponding IC_{50} values obtained against SHP2, as determined by ANOVA/Dunnett's test; [b] Reported IC_{50} value against SHP2 in a similar DiFMUP assay protocol using fl-SHP2 enzyme and a bis-tyrosyl phosphorylated peptide activator [94].

SAR of SHP2 inhibition for compounds STS01-STS25

The library of 25 compounds consists of analogous members containing two variable centres A and B (**Figure 3.4**), one being the aryl/heteroaryl ring (centre A) attached to the thiadiazole core and other being the heterocyclic ring extension (centre B). Combinative structural modifications at both the centres display appreciable effect on the IC_{50} values of the compounds of the series.

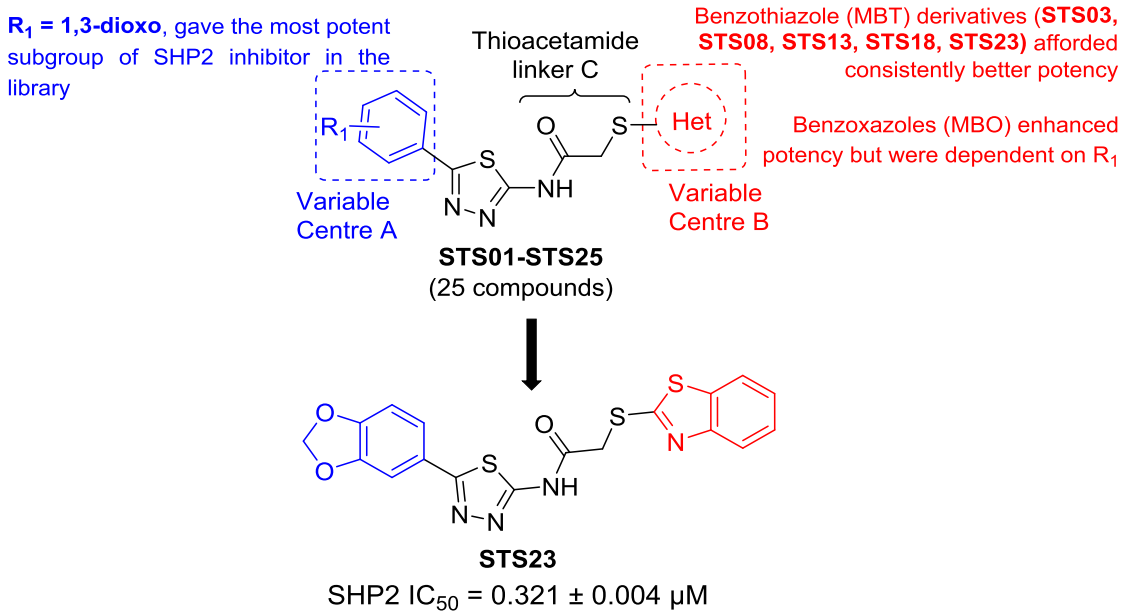

Figure 3.4. Structure-activity relationship (SAR) of the synthesized compounds **STS01-STS25** along with the structure of most potent compound **STS23**. All correlating statements in the figure are with reference to the corresponding unsubstituted analogue i.e. R_1 = H and R_2 = H wherever applicable.

A study of the IC_{50} values of all the tested compounds gives us an idea regarding the correlation between the various structural modifications attempted on our designed scaffold and their activity against SHP2 and are listed below:

- Most notable among the structure-activity relationship analysis is the effect of introducing the 1,3-benzodioxo group at centre A which gave some of the most

potent compounds of the series (viz. **STS23, STS22, STS21**) with the most potent one compound **STS23** (0.321 μM).

- Among the non-substituted derivatives, i.e., (**STS01-STS05**) R_1 = H, the most potent compound was found to be the corresponding benzimidazole homologue with an IC_{50} of 0.915 μM whereas the other compounds of this cluster were moderate in their SHP2 inhibition.

- The corresponding 4-fluoro derivatives (i.e., **STS06-STS10**) were all more potent than the unsubstituted analogues (**STS01-STS05)** indicating desirable effects of the 4-fluoro substitution on the activity of the resultant compounds.

- The 4-methoxy cluster (**STS11-STS15**) however, showed mixed type of activity profile with the activity depending ultimately on the type of heterocyclic appendage in the molecule. For e.g., **STS11** (IC_{50} = 0.842 μM) was more potent than other molecules of this cluster which has a 5-methyl-1,3,4-thiadiazole moiety making it essentially a homodimeric hybrid of the 1,3,4-thiadiazole ring tethered by the thioacetamide linker.

- The next cluster belonging to the R_1 = 3,4-dimethoxy group derivatives (**STS16-STS20**), also showed similar activity profiles ; however, here, the most potent compound was the corresponding benzothiazole derivative (**STS18**, IC_{50} = 0.737 μM).

- For the 1,3-benzodioxole derivatives i.e., R_1 = 1,3-dioxonium group (**STS21-STS25**), activity profile was similar to the other groups but here, the most potent compound of the series was obtained (compound **STS23,** IC_{50} = 0.321 μM).

- Among the heterocyclic core effects, the benzothiazole analogues (i.e. Het = MBT) afforded consistently better potency (viz. **STS03, STS08, STS13, STS18, STS23**).
- The benzoxazoles (i.e., Het = MBO) also enhanced SHP2 inhibitory activity but were dependent on the corresponding R_1 group, e.g., only the 4-fluoro MBO derivative (**STS07)** and the benzodioxo MBO derivative (**STS22)** were potent among the subgroup.
- The 2-methylmercaptotetrazole derivatives (i.e. Het = MMT) showed decreased potency against the enzyme due to their smaller size (viz. **STS05, STS10, STS15, STS20, STS25**).

3.3.2.2. *In vitro* antioxidant assay

The foremost five molecules that exhibited the best anti-SHP2 activity were subjected to an antioxidant activity assay using DPPH protocol to correlate their *in vitro* anti-SHP2 & anticancer potential with their antioxidant property. Ascorbic acid (AA) was used as the positive control. The antioxidant activity of the compounds is reported as IC_{50} value and percent free radical scavenging (% FRS) activity in **Table 3.3** and the % FRS is also given in **Figure 3.5** as a plot vs. concentration of the respective compound in μM. All the tested compounds demonstrated moderately potent antioxidant activity as compared to ascorbic acid (DPPH IC_{50} = 67.23 ± 0.824 μM) with compound **STS23** being the most potent one (DPPH IC_{50} = 87.38 ± 0.45 μM).

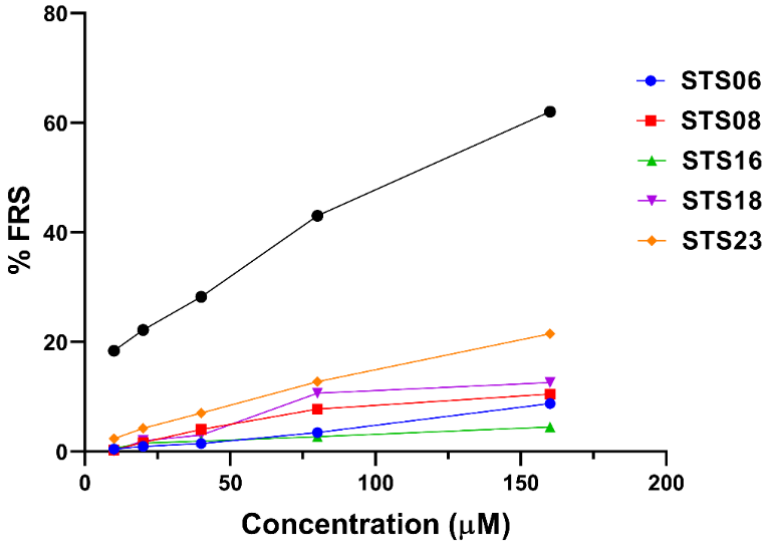

Figure 3.5. Percent free radical scavenging (% FRS) activity of compounds **STS06**, **STS08, STS16, STS18, STS23** and ascorbic acid plotted against the various concentrations of each compound used in the assay. The individual plot points represent the % FRS value obtained from two independent experiments in triplicate, expressed as mean ± SEM.

Table 3.3. Antioxidant activity of compounds of **STS series** by DPPH assay

Compd	Antioxidant activity (DPPH assay)	
	% FRS[a]	**IC_{50} (μM)[b]**
STS06	9.7	109.70 ± 0.68
STS08	7.9	143.95 ± 1.03
STS16	5.5	177.87 ± 6.25
STS18	8.9	123.20 ± 1.86
STS23	15.1	82.38 ± 0.45
Ascorbic acid[c]	67.23 ± 0.82	62.50 ± 0.62

[a] % Free radical scavenging (FRS) activity at 100 μM compound concentration.
[b] Mean IC_{50} of two independent experiments assayed in triplicate each ± SEM.
[c] Used as positive control.

3.3.2.3. *In vitro* blood-brain barrier permeability assay (PAMPA-BBB) of compound STS23

The in vitro BBB permeability assay of compound **STS23** was performed and the effective permeability (P_e) value obtained from the assay is given in **Table 3.4**.

Compound **STS23** displayed a P_e value of (3.117 ± 0.097) $\times 10^{-6}$ cm/s after an incubation of 18 h. According to Di et.al., any molecule is CNS+ if its $P_e > 4.0 \times 10^{-6}$ cm/s, is CNS± if its $P_e > 2.0 \times 10^{-6}$ cm/s $< 4.0 \times 10^{-6}$ cm/s and is CNS- when $P_e < 2.0 \times 10^{-6}$ cm/s [147]. Thus, this indicates an ambiguous CNS permeability index i.e., compound **STS23** is a probable CNS± molecule. In other words, it may or may not cross the BBB as shown by the corresponding *in vitro* experiment.

Table 3.4. PAMPA-BBB assay data

Compd	P_e ($\times 10^{-6}$ cm/s)[a]	Reference P_e ($\times 10^{-6}$ cm/s)[b]	Predicted BBB[c]	CNS Category[d]	Reported CNS[b]
STS23	3.117 ± 0.097	NA	0.018	CNS±	NA
Docetaxel	2.687 ± 0.320	NA	0.025	CNS±	NA
Imipramine[e]	14.922 ± 0.131	13	2.920	CNS+	CNS+
Tenoxicam[e]	1.267 ± 0.168	0.1	0.095	CNS-	CNS-

[a] P_e values as mean ± SD of two independent experiments in duplicate.

[b] Values are cited from Di *et.al.*, 2003 [147].

[c] BBB permeability using PreADMET web-based server (accessed on 08.08.2024).

[d] CNS+ ($P_e > 4.0 \times 10^{-6}$ cm/s), CNS± ($P_e > 2.0 \times 10^{-6}$ cm/s $< 4.0 \times 10^{-6}$ cm/s), CNS- ($P_e < 2.0 \times 10^{-6}$ cm/s)[b]

[e] Used as positive and negative permeability controls respectively.

NA: not applicable

3.3.2.4. Cell-based assays

3.3.2.4.1. Cell proliferation assay using MTT

The synthesized compounds were assayed by an MTT assay by incubating with the suitable cells for 3-5 days. The cell plate was detected with the help of MTT reagent. The results of the inhibitory activity of the tested compounds are shown in **Table 3.5**. All the tested compounds displayed moderate antiproliferative activity against cell lines of various cancers like human breast cancer, rat phaeochromocytoma, and human glioblastoma. The antiproliferation activity of compound **STS23** was 39% at a

concentration of 100 μM for PC12 cell lines and 51% at a concentration of 100 μM for U87MG cell lines.

The compounds **STS09** and **STS08** consisting of a para-fluorophenyl substitution at R_1 of site A (**Figure 3.4**) showed the best-in-library antiproliferative activity for MCF-7 cells (MCF-7 IC_{50} = 98.27 ± 1.45 μM and 105.0 ± 1.54 μM respectively). However, the lead SHP2 inhibitor **STS23**, having benzodioxole substitution at site A showed moderate antiproliferative activity for MCF-7 cells with an IC_{50} value of 134.5 ± 0.630 μM. Further, the antiproliferative activity of compound **STS23** was tested in PC12 and U87MG cell lines and was found to be 39% at a concentration of 100 μM for PC12 cell lines (IC_{50} = 39.99 ± 0.120 μM) and 51% at a concentration of 100 μM for U87MG cell lines (IC_{50} = 94.32 ± 0.258 μM), as depicted in **Table 3.5**.

Figure 3.6 shows the percent cell viability versus concentration plot of compound **STS23** for MCF-7, PC12 and U87 cells. The plots illustrate that the compound has significant cytotoxicity for all the cells as compared to the control group that becomes dose-dependent at a concentration of 70 μM or more. In absolute terms, the observation indicates low to moderate cytotoxicity of compound **STS23** against the MCF-7 and PC12 cells with an approximate cell viability of 50% at a concentration of 100 μM. For U87MG cells, compound **STS23** has highly significant ($p<0.0001$) cytotoxicity as compared to the control group. The cytotoxicity becomes dose-dependent beyond a dose of 250 μM and gradually differing lower doses produced strong but consistent cytotoxicity (approximately 50% cell viability) as seen from the plot of **Figure 3.6C**. All data represented in the plot are mean of three individual experiments along with the corresponding standard error of mean.

Figure 3.6D shows the inverted microscopic images of MCF-7, PC12 and U87MG cells treated with compound **STS23** at a concentration of 0 μM (control) and 50 μM (for MCF-7) and 100 μM (for PC12 and U87MG), The images illustrate the morphological changes caused by the treatment of the respective cells with the test compound for a period of 24 h as compared to control group. As seen from the first and second panels, the MCF-7 cells were sufficiently lysed with substantial loss of morphology with the appearance of apoptotic bundles (the black clusters seen in the second panel) on treatment with the compound at a concentration of 50 μM for 24 h. In the third and fourth panel too, significant loss of viable cells as well as the homeostatic morphology was seen post-treatment. Similarly, U87MG astrocytes on treatment with compound **STS23** at a concentration of 100 μM for a period of 24 h showed drastic decrease in the astrocytes as compared to control group as seen from the fifth and sixth panel of **Figure 3.6D**. The cell morphology and behaviour could also be visualized to have changed post-treatment with compound **STS23** for the U87MG astrocytes. The observed results inferred that the mortality of SHP2-driven GBM cells like U87MG as well as neural and breast cancer cells has direct correlation with the SHP2 inhibitory effect of compound **STS23**.

A quick comparison of the *in vitro* SHP2 inhibitory activity of the compounds of **STS series** (**Table 3.2**) and their MCF-7 antiproliferative activity (**Table 3.5**) was done to draw any correlation between these two activities. It was inferred from the comparison that most compounds of the series displayed moderate antiproliferation activity which was not directly dependent on their corresponding SHP2 inhibitory activity and thus, in turn on the substituents present in the molecules. As exceptions, compound **STS09**, the cellular lead compound (MCF-7 GI_{50} = 98.57 μM) was a moderately potent

submicromolar SHP2 inhibitor (IC_{50} = 0.859 μM) and compound **STS08** with an SHP2 IC_{50} of 0.540 μM and MCF-7 GI_{50} of 105 μM showed comparable and balanced activity in both the assays emerging as a kind of balanced lead. Our *in vitro* lead SHP2 inhibitory compound **STS23** showed moderate antiproliferation activity as has already been discussed above.

Table 3.5. Growth inhibition data (GI_{50}) of tested compounds of **STS series**

Compd	GI_{50} (μM)		
	MCF-7	**PC12**	**U87MG**
STS03	> 2000	NT	NT
STS04	548.2 ± 4.55	NT	NT
STS06	150.4 ± 2.43	NT	NT
STS07	129.5 ± 2.13	NT	NT
STS08	105.0 ± 1.54	NT	NT
STS09	98.27 ± 1.45	NT	NT
STS11	180.4 ± 0.24	NT	NT
STS12	223.6 ± 6.27	NT	NT
STS14	> 2000	NT	NT
STS16	165.7 ± 2.11	NT	NT
STS18	209.5 ± 1.32	NT	NT
STS20	140.5 ± 3.22	NT	NT
STS21	445.0 ± 7.53	NT	NT
STS22	296.8 ± 1.72	NT	NT
STS23	134.5 ± 0.63	39.99 ± 0.12	94.32 ± 0.26
STS25	187.1 ± 3.69	NT	NT
Docetaxel[a]	4.84 ± 0.16	NT	NT

[a] Reference standard for MTT assay on MCF-7 cells; NT: Not tested

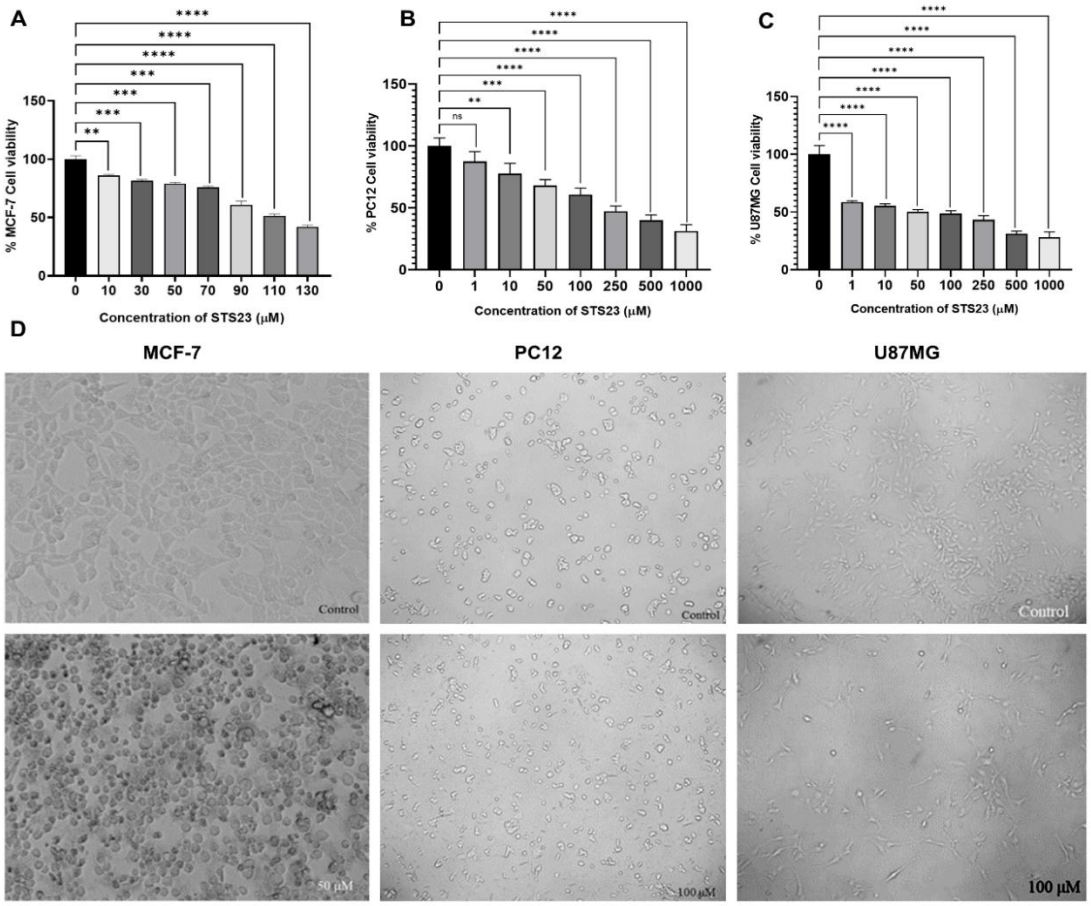

Figure 3.6. *In vitro* cytotoxicity of compound **STS23** on human breast cancer cells (MCF-7), rat-derived neural phaeochromocytoma cells (PC12), and human glioblastoma cells (U87MG) after 24 h. A) Percent cell viability vs. concentration graph of compound **STS23** for MCF-7 cells. Mean ± SEM (n = 3). $p<0.0001$. B) Percent cell viability vs. concentration graph of compound **STS23** for PC12 cells. Mean ± SEM (n = 4). $p<0.0001$. C) Percent cell viability vs. concentration graph of compound **STS23** for U87MG cells. Mean ± SEM (n = 4). $p<0.0001$. D) Inverted microscopic image of MCF-7, PC12 and U87MG cells treated with compound **STS23** at 0 μM (control) and 100 μM concentrations (50 μM in case of MCF-7).

3.3.2.4.2. Colony formation assay of compound STS09 and STS23

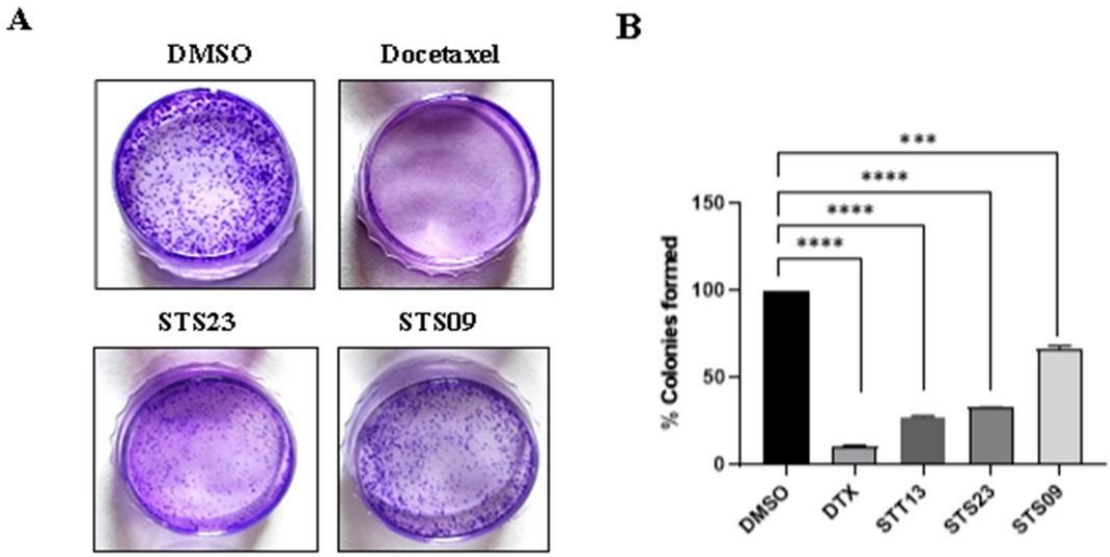

Figure 3.7. A) Inhibition of colony formation of MCF-7 cells by compounds **STS09** and **STS23** and docetaxel (reference standard) as compared to untreated cells (DMSO control) after an incubation of 7 days. B) Histogram quantifying the % colony formed (n = 3). ** P < 0.01, *** P < 0.001 versus DMSO.

Compounds **STS09** and **STS23** were evaluated for their effect on the proliferation capacity of MCF-7 cells through a colony formation assay as described earlier [155]. Compound **STS23** showed moderate inhibition of colony growth of MCF-7 cells as seen by crystal violet staining of the cells upon an incubation of 7 days (**Figure 3.7A**). Docetaxel was used as the internal standard. Treatment with 5 μM of compound **STS23** resulted in a significant decrease in the clonogenic number and formation rate of U87MG cells (**Figure 3.7B**). Compound **STS09,** though a strong cytotoxic, did not inhibit MCF-7 colony formation very strongly.

3.3.2.5. *In vivo* studies

3.3.2.5.1. Acute oral toxicity study in female Wistar rats

Encouraged by the acceptable *in vitro* efficacy of compound **STS23** against SHP2 enzyme and MCF-7 cells, it's *in vivo* safety was evaluated by conducting an acute oral

toxicity study on adult female Wistar rats in accordance with the OECD Guideline 423 (Acute Toxic Class Method)[132] to determine its median lethal dose i.e., LD_{50}. No animal was found dead or in moribund state within or after 14 days at the highest dose of 2000 mg/kg body weight (BW) indicating compound **STS23** was safe for all the animals with its LD_{50} being >2000 mg/kg. Further, no external signs of toxicity were observed in any animal nor in the first 4 h post dosing neither in the subsequent 14 days; the vital signs and behavioural pattern of all groups were also normal (**Table 3.6**). The body weight parameter of the animals in the test and control groups were determined and statistical analysis by two-way ANOVA revealed no significant differences in the body weight among the groups ([$F(2,45) = 2.661$; $p > 0.05$]), time ([$F(2,45) = 1.433$; $p > 0.05$]) and their interaction ([$F(4,45) = 0.05848$; $p > 0.05$]).

Table 3.6. General observation and behavioural analysis during the first 4 h and 24 h after single-dose administration of compound **STS23** (300 mg/kg BW & 2000 mg/kg BW) in female Wistar rats (n = 6 female rats/group).

Observations	**Control**		**STS23 (300 mg/kg)**		**STS23 (2000 mg/kg)**	
	4 h	**24 h**	**4 h**	**24 h**	**4 h**	**24 h**
Skin and fur	NC	NC	NC	NC	NC	NC
Eyes	NC	NC	NC	NC	NC	NC
Mucous membrane	NC	NC	NC	NC	NC	NC
Salivation	NC	NC	NC	NC	NC	NC
Diarrhoea	NO	NO	NO	NO	NO	NO
Lethargy	NO	NO	NO	NO	NO	NO
Sleep	N	N	N	N	N	N
Coma	NO	NO	NO	NO	NO	NO
Tremors and convulsions	NO	NO	NO	NO	NO	NO
Behaviours pattern & somatosensory activity	N	N	N	N	N	N

Note: N-normal, NO-not observed, NC-no change

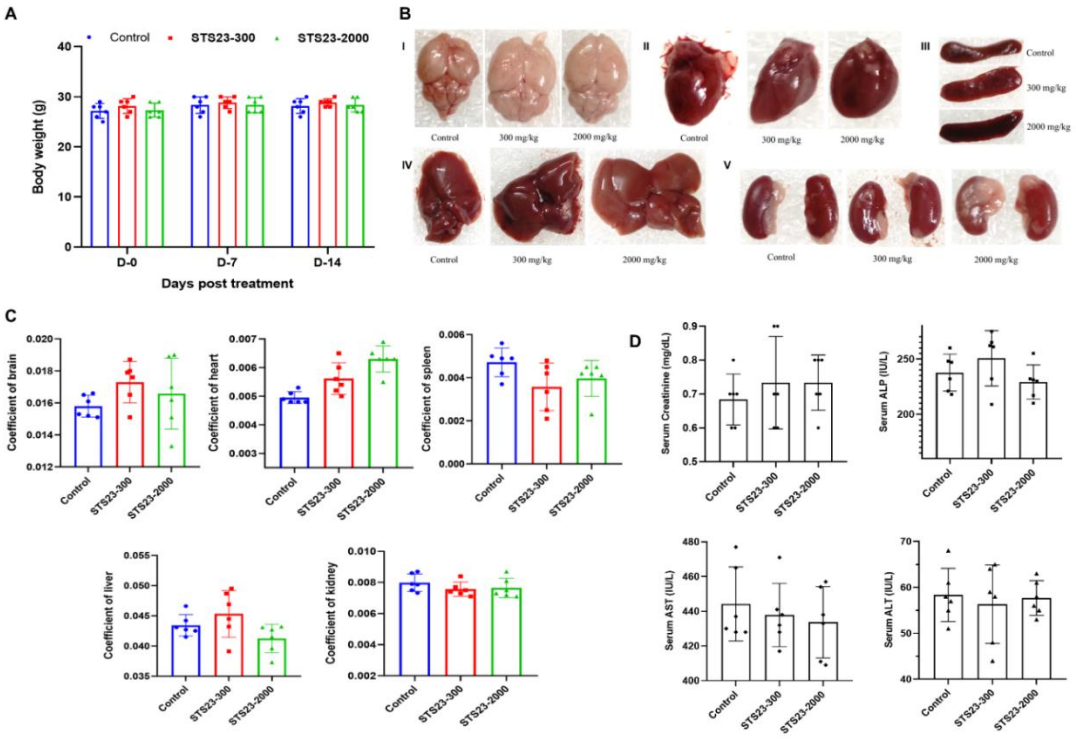

Figure 3.8. Acute oral toxicity study of compound **STS23** in adult female albino mice (in accordance with OECD Guidelines 423). A) Effect of single-dose oral administration of compound **STS23** (at two doses of 300 mg/kg BW and 2000 mg/kg BW) on (I) body weight of mice at pre-treatment, Day-7 and Day-14. (Two-way ANOVA followed by Bonferroni post hoc test). B) Representative macroscopic photographs showing normal morphology of brain (I), heart (II), kidneys (III), liver (IV) and spleen (V) of animals after single-dose administration of vehicle (control) and 300 mg/kg BW & 2000 mg/kg BW of compound **STS23** at the end of day 14. C) Effect of single-dose oral administration of compound **STS23** (300 mg/kg BW and 2000 mg/kg BW) on organ coefficient of the brain (I), heart (II), liver (III), kidneys (IV), and spleen (V) at the end of the experiment. D) Effect of single-dose oral administration of compound **STS23** (300 mg/kg BW and 2000 mg/kg BW) on serum concentration of creatinine (I), ALP (II), AST (III) and ALT (IV) at the end of the experiment. All values are in mean ± SD (n = 6 female rats/group). (One-way ANOVA followed by Tukey's multiple comparison post hoc test).

The effect of single-dose oral administration of compound **STS23** (300 mg/kg & 2000 mg/kg BW) on the organ coefficient of vital organs i.e., brain, heart, liver, kidneys and spleen were determined post sacrifice of the animals and is depicted in **Figure 3.8C**. From the figure we can see that compound **STS23** does not cause any significant changes in the organ coefficient of these highly perfused organs in any of the groups (statistical analysis by one-way ANOVA revealed no significant changes in the organ

coefficient of brain, heart, liver, kidneys, and spleen among the groups; [F(2,15) = 1.439; p > 0.05], [F(2,15) = 1.217; p > 0.05], [F(2,15) = 3.163; p > 0.05], [F(2,15) = 0.9502; p > 0.05], and [F(2,15) = 2.566; p > 0.05] respectively) indicating that compound **STS23** is safe for the organs even at the highest test dose of 2000 mg/kg BW. Furthermore, the macroscopic evaluation of the said organs of all groups (**Figure 3.8B**) were comparable and did not show any toxicological effects on the perfused organs of all the three groups.

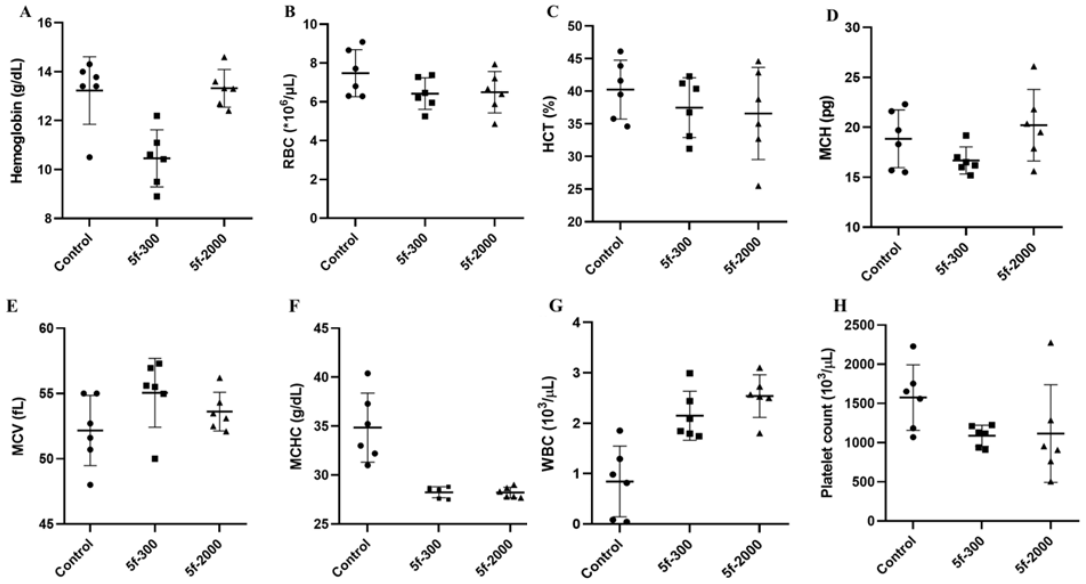

Figure 3.9. Effect of single-dose oral administration of compound **STS23** (300 & 2000 mg/kg BW) on CBC of female albino mice at the end of 14-day experimental protocol. All values are in mean ± SD (n=6 female mice/ group). (One-way ANOVA followed by Tukey's multiple comparison post hoc test).

Further, it can be seen from the photomicrographs shown in **Figure 3.10** a single oral administration of a dose 2000 mg/kg BW of compound **STS23** exhibited no damage to the tissue architecture of the brain, liver, heart, spleen and the kidneys with no histopathological changes in any of these highly perfused organs at the end of the experiment i.e., on the 14th day.

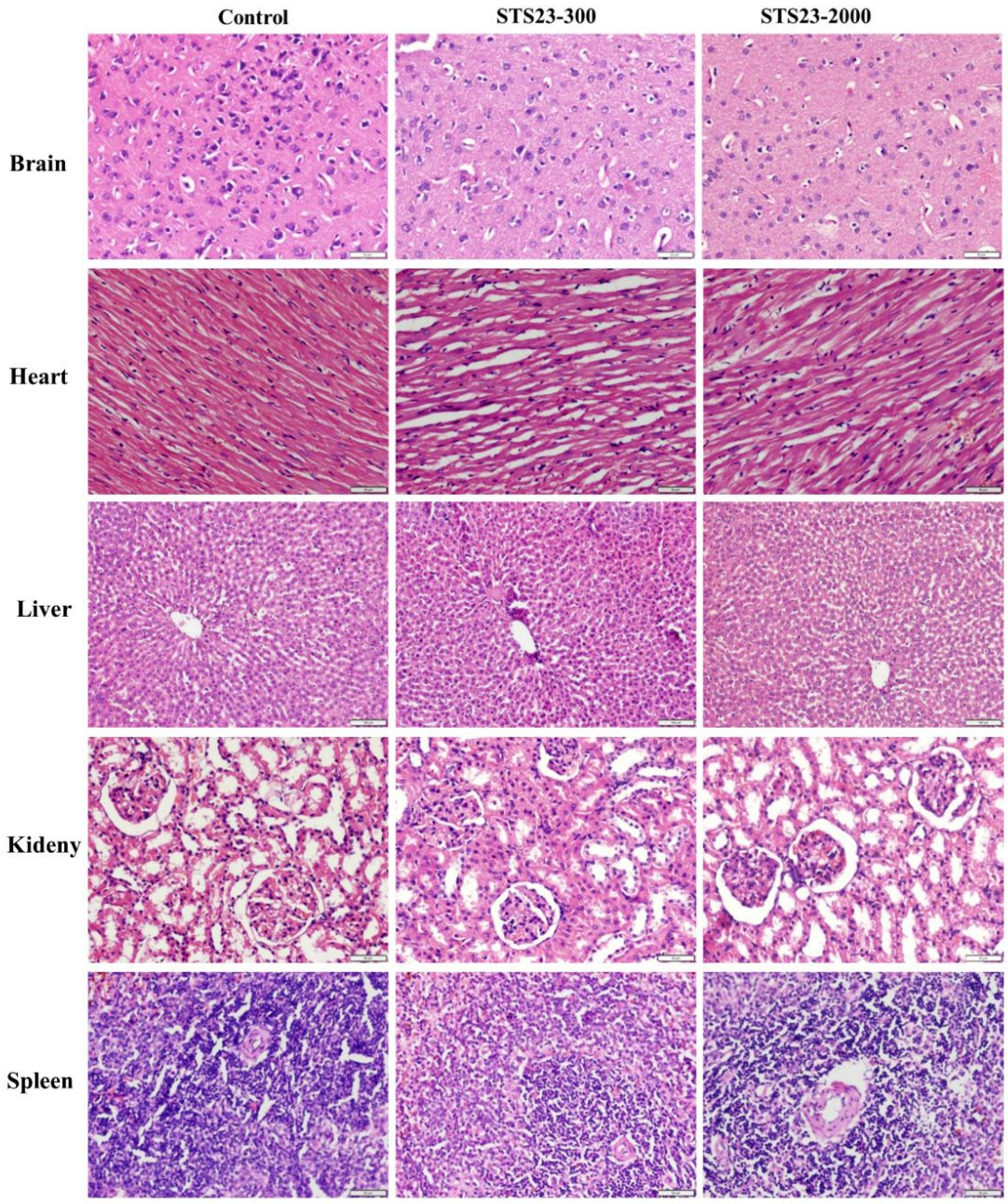

Figure 3.10. A) Effect of single-dose oral administration of compound **STS23** (at a dose of 2000 mg/kg BW) along with vehicle control on brain of female Wistar rats and B) on other highly perfused organs viz. heart, liver, kidney, and spleen tissue stained with hematoxylin and eosin (H&E) dye at the end of 14 days.

Next, we evaluated the toxicological effect of our test compound **STS23** on the biochemical and haematological parameters of the animals All measurements and statistical data of the biochemical measurements for serum creatinine (mg/dL), ALP

(IU/L), AST (IU/L) and ALT (IU/L) are shown in **Figure 3.8D**. We can observe from the figure that there were no substantial changes in the serum level of the enzymes in any of the groups when compared to control (statistical analysis by one-way ANOVA revealed no significant changes in the serum level of creatinine, AST, ALT, and ALP among the groups; [$F(2,15) = 0.4839$; $p > 0.05$], [$F(2,15) = 0.4151$; $p > 0.05$], [$F(2,15) = 0.1545$; $p > 0.05$], and [$F(2,15) = 1.851$; $p > 0.05$] respectively). Lastly, complete blood count (CBC) of all the test groups (parameters tested were hemoglobin, red blood cell count (RBC), hematocrit (HCT), mean corpuscular hemoglobin (MCH), mean corpuscular volume (MCV), mean corpuscular hemoglobin concentration (MCHC), red blood cell distribution width (RDW), platelet count and white blood cell count (WBC), **Figure 3.9**) after single-dose oral administration of compound **STS23** showed no significant changes or deviations from the control group. From the above findings of the toxicological study, we inferred that the compound is nontoxic and safe at the high oral dose of 2000 mg/kg BW.

3.3.3. Computational studies

3.3.3.1. Molecular docking of compounds STS01-STS25 within the tunnel allosteric site of SHP2 (PDB ID: 5EHR)

Molecular docking studies of compounds **STS01-STS25** in the tunnel allosteric site of SHP2 (PDB ID: 5EHR) was performed by AutoDockTools 4.2 software using a validated protocol with **SHP099** as the co-crystallized ligand**.** The 3D superimposition image of all compounds of the **STS series** is given in **Figure 3.11** where the compounds have been grouped into specific cluster depending on the substitution at the phenyl ring on the 1,3,4-thiadiazole ring (i.e., variable site A). The superimposition pattern reveals that all 25 compounds are well lodged in the tunnel allosteric site of 5EHR having

appreciable overlap with co-crystallized ligand **SHP099** (PDB ID: 5OD). However, few molecules bifurcate slightly from the orientation of **SHP099** and move towards the PTP domain residues (**STS18, STS19, STS22**) (**Figures 3.11D** & **3.22E**).

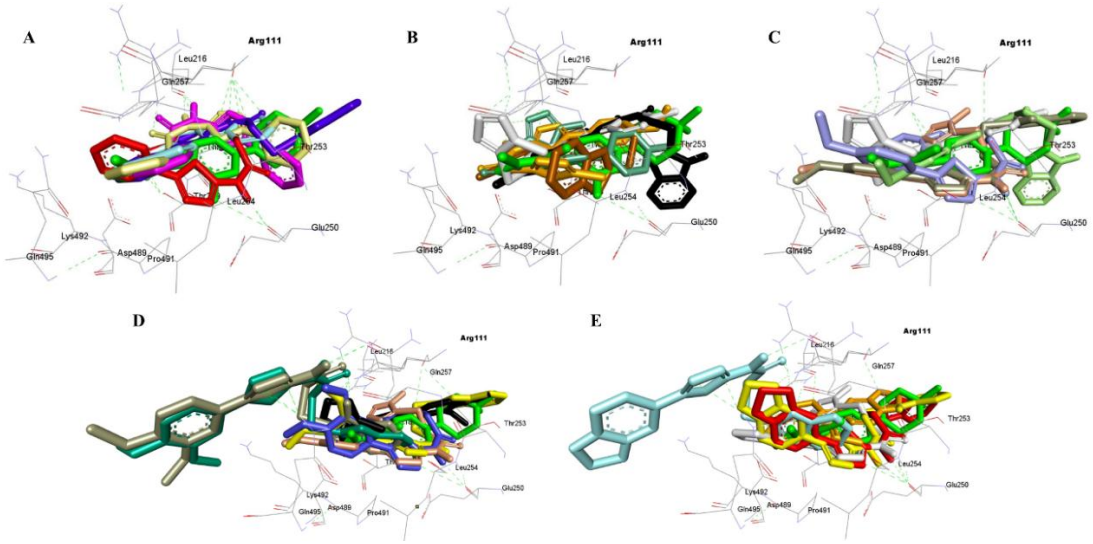

Figure 3.11. 3D superimposition image of **STS series** of compounds in SHP2 (PDB ID: 5EHR) for A) compounds **STS01-STS05**, B) compounds **STS06-STS10**, C) compounds **STS11-STS15**, D) compounds **STS16-STS20** and E) compounds **STS21-STS25.**

Table 3.7. Molecular docking data of compounds **STS01-STS25**

Compd Code	ΔG (Kcal/mol)	K_i (nM)	Compd Code	ΔG (kcal/mol)	K_i (nM)
STS01	-9.96	49.69	**STS14**	-9.24	167.42
STS02	-9.98	48.22	**STS15**	-9.78	67.23
STS03	-9.61	89.62	**STS16**	-10.45	21.92
STS04	-9.09	218.19	**STS17**	-9.39	130.53
STS05	-9.71	75.83	**STS18**	-9.90	55.66
STS06	-9.05	232.35	**STS19**	-9.44	119.74
STS07	-9.17	189.90	**STS20**	-10.26	30.12
STS08	-9.70	77.52	**STS21**	-9.57	96.95
STS09	-9.49	110.21	**STS22**	-10.13	37.36
STS10	-10.09	40.07	**STS23**	-9.95	50.52
STS11	-9.63	86.01	**STS24**	-10.52	19.51
STS12	-9.45	118.78	**STS25**	-10.09	39.93
STS13	-9.67	81.63	**SHP099**	-10.27	29.34

[a] K_i calculated from the binding energy of poses generated by AutoDockTools 4.2.

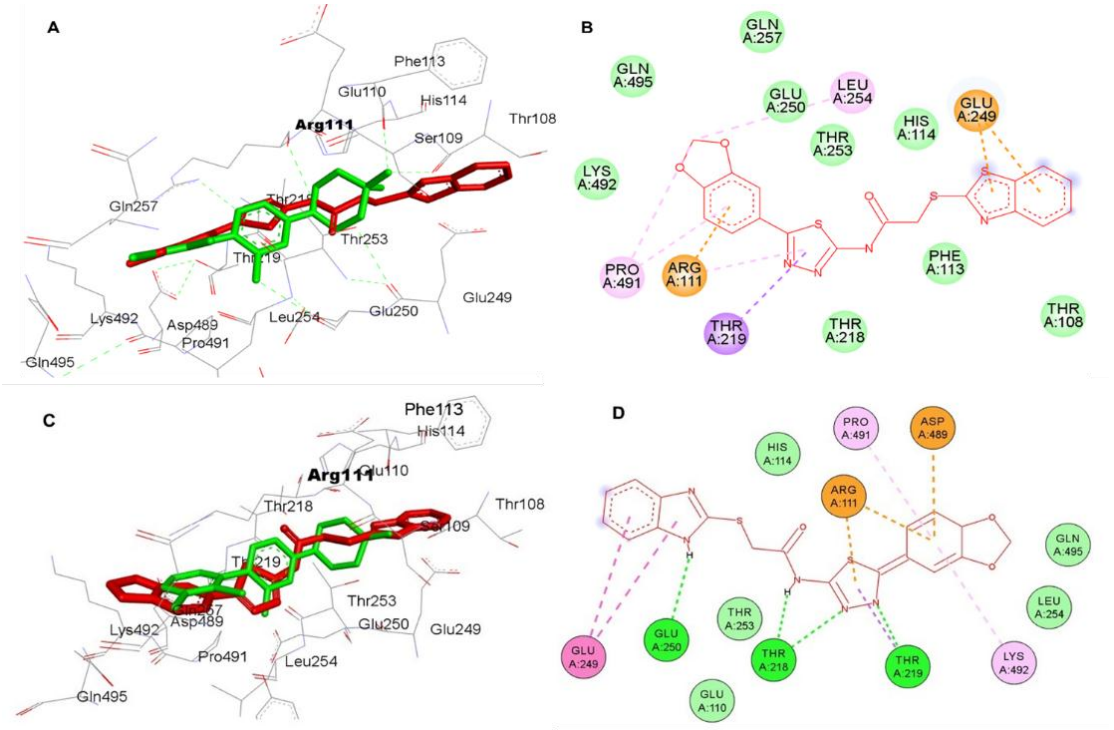

Figure 3.12. A) 3D orientation image of compound **STS23** (red) with **SHP099** (green) in the tunnel allosteric site of 5EHR; B) 2D interaction map of compound **STS23** (red) with **SHP099** (green) in the tunnel allosteric site of 5EHR; C) 3D orientation image of compound **STS24** (red) with the amino acid residues of the tunnel allosteric site of 5EHR, D) 2D interaction map of compound **STS24** (red) with the amino acid residues of the tunnel allosteric site of 5EHR.

A. Binding data of compound STS23 within the crystal structure of 5EHR

In SHP2 tunnel allosteric site, compound **STS23** occupies the central cavity that is occupied by the co-crystallized ligand 5OD with a near perfect overlap with it. As can be seen from **Figure 3.12A**, the central 1,3,4-thiadiazole ring superimposes with the central piperidine ring and the terminal 3,4-dimethoxyphenyl ring overlaps the pyrazine ring of compound **SHP099**. Also, the planar dichlorophenyl ring of **SHP099** is almost flanking the same region occupied by the benzimidazole ring of compound **STS23**. **Figure 3.12B** shows the 2D interaction pattern of compound **STS23** in SHP2.

B. Binding data of compound STS24 within the crystal structure of 5EHR

Visual inspection of the 3D orientation of compound **STS24** in the tunnel allosteric site of SHP2 (**Figure 3.12C** and **3.12D**) reveal several features that explain its high binding affinity with SHP2. The compound is well accommodated within the gorge and superimposes nicely with 5OD, the native ligand. The molecule orients itself in a manner that its extremities are exposed to the receptor sites. The central thiadiazole ring of compound **STS24** overlaps with the central pyrimidine ring of **SHP099** whereas the planar piperonyl ring orients towards the planar phenyl ring possibly with a pi-pi stacking interaction. However, the molecule is wider than **SHP099** due to which its benzimidazole moiety juts out of the cavity with the thioether linker superimposing with the saturated carbocycle of **SHP099**. The 2D interaction image shows that the 1,3,4-thiadiazole ring of compound **STS24** interacts with Arg111 via a strong arene-hydrogen bonding which is crucial for better binding affinity. Additionally, nitrogen atom of the benzimidazole ring interacts with Thr108 by hydrogen bonding where the -NH acts as a donor towards the threonine carbonyl oxygen.

3.3.3.2. Molecular dynamics simulation studies for compound STS23

Molecular dynamics simulation was performed on compound **STS23** with the help of Desmond molecular dynamics software (Schrodinger Release 2021.1) to assess the compound's binding pattern to the tunnel allosteric site of SHP2 enzyme model (PDB ID: 5EHR) and to establish the effects of the simulated allosteric binding on the protein molecule structure (**Figure 3.13**). The simulation was run for 100 ns at 300 K temperature and Maestro graphical user interface (Maestro, Schrodinger, LLC, New York, NY, 2021) was employed to analyse and visualize the outcomes. The *in silico*

study shows that compound **STS23** interacted with several amino acid residues of tunnel allosteric site of SHP2 via H-bonding and hydrophobic interactions and enhanced the stability of the enzyme on binding.

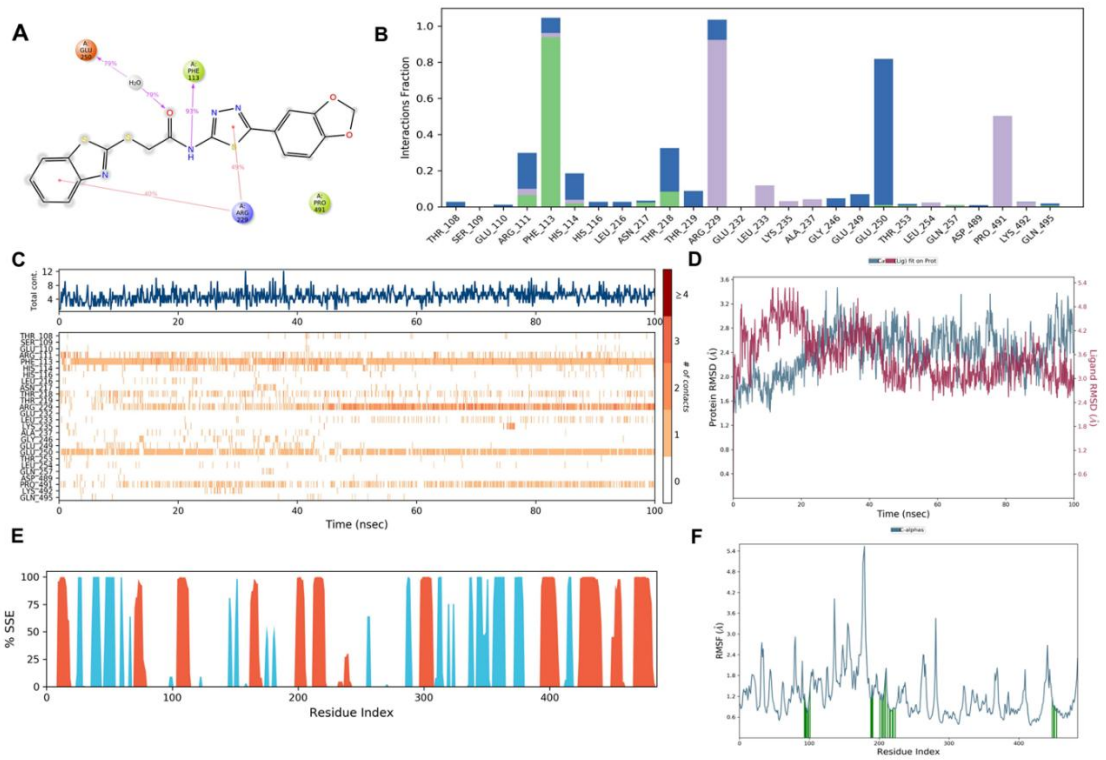

Figure 3.13. Protein-ligand contact diagrams ('simulation interactions diagrams') generated through Molecular Dynamics simulation of compound **STS23** with SHP2 (PDB ID: 5EHR). A) Percent interaction of ligand with protein (represented by purple arrow). B) Stacked bar chart representing different types of protein-ligand contacts. C) Protein-ligand contacts in timeline representation for 100 ns simulation; D) Protein-ligand RMSD graph. E) Protein secondary structure elements (SSE) plot; F) Protein RMSF graph shown in blue.

3.3.3.3. Predicted ADMETox parameters

The ADMETox properties of the final compounds **STS01-STS25** were predicted by Pre-ADMET online server (https://preadmet.webservice.bmdrc.org/, accessed on 23rd November 2022). The predicted ADME and toxicological properties of all compounds are given in **Tables 3.8** and **3.9** respectively. All compounds displayed similar skin

permeability with a value around -4. An analysis of the values shows that all compounds have low BBB penetrability with moderate to high plasma-protein binding.

Table 3.8. Predicted ADME properties of compounds **STT01-STT21**

Compd Code	MW	CLogP	HIA (%)	Caco2	MDCK (nm/s)	SP (logKp, cm/h)	BBB	PPB (%)	CYP2C9	CYP 2C19	CYP 3A4
STS01	349.44	1.8836	91.08	1.67	1.2335	-4.01	0.079	84.61	non	non	weak
STS02	368.43	3.7086	98.25	9.61	5.259	-3.62	0.196	89.87	non	non	non
STS03	384.49	4.3876	98.62	15.86	13.647	-3.39	0.206	96.79	non	non	non
STS04	367.44	3.8586	92.25	6.87	6.2230	-4.303	0.064	93.20	inhibitor	non	non
STS05	333.38	1.6666	87.68	0.562	5.3072	-4.183	0.065	78.96	non	non	weakly
STS06	367.44	2.0299	91.15	1.667	1.367	-4.23	0.089	84.41	non	non	weak
STS07	386.42	3.8549	98.26	10.52	1.980	-3.90	0.243	89.40	non	non	non
STS08	402.48	4.5339	98.63	16.61	1.995	-3.70	0.251	94.17	non	non	non
STS09	385.43	4.0049	92.27	7.481	2.0672	-4.537	0.085	91.48	inhibitor	non	Non
STS10	351.38	1.8129	87.79	0.558	8.0252	-4.379	0.074	80.65	non	non	weakly
STS11	379.47	1.9421	89.12	2.84	1.019	-4.20	0.074	82.68	non	non	non
STS12	398.55	3.7671	97.85	14.16	1.524	-3.79	0.177	88.90	non	non	non
STS13	414.46	4.4461	98.24	21.23	0.998	-3.62	0.182	94.95	non	non	non
STS14	397.47	3.9171	92.32	10.251	1.5285	-4.470	0.049	90.99	inhibitor	non	non
STS15	363.44	1.7251	85.11	0.671	6.2870	-4.358	0.064	76.96	non	non	weakly
STS16	409.49	1.6649	86.91	4.08	0.243	-4.34	0.063	79.28	non	non	weak
STS17	428.48	3.4899	97.19	17.18	1.751	-3.93	0.132	89.91	non	non	non
STS18	444.54	4.1689	97.61	24.34	4.594	-3.79	0.134	93.94	non	non	non
STS19	427.49	3.6399	92.54	12.996	2.5417	-4.553	0.035	91.43	inhibitor	non	non
STS20	393.44	1.4479	82.23	0.788	0.8326	-4.483	0.057	72.50	non	non	substrate
STS21	393.45	1.9719	85.49	3.048	0.5443	-4.572	0.056	81.13	non	non	non
STS22	412.44	3.7969	96.76	7.801	2.445	-4.302	0.109	92.29	non	non	non
STS23	428.50	4.4759	97.24	13.908	0.762	-4.199	0.111	97.35	non	non	non
STS24	411.49	3.9469	92.44	3.586	2.423	-4.872	0.029	95.33	inhibitor	non	non
STS25	377.39	1.7549	80.22	0.822	2.102	-4.661	0.053	75.93	non	non	substrate

HIA: Human Intestinal Absorption [0–20 (poor), 20–70 (moderate), 70–100 (well)], **Caco2**: In-vitro Caco2 cell permeability [<4 (low), 4–70 (moderate), >70 (high)], **MDCK**: Maden Darby Canine Kidney cell permeability [<25 (low), 25–500 (moderate), >500 (high)], **SP**: Skin permeability, **BBB**: Blood brain barrier permeability (C_{brain}/C_{blood}), **PPB**: In-vitro plasma protein binding.

Table 3.9. Predicted toxicological properties of compounds **STS01-STS25**

Compd code	Ames test	Carcinogenicity (Mouse)	Carcinogenicity (Rat)	hERG Inhibition
STS01	mutagen	negative	negative	medium risk
STS02	mutagen	negative	negative	low risk
STS03	mutagen	negative	positive	low risk
STS04	mutagen	negative	positive	high risk
STS05	mutagen	negative	positive	medium risk
STS06	mutagen	negative	negative	medium risk
STS07	mutagen	negative	negative	low risk
STS08	mutagen	negative	positive	low risk
STS09	mutagen	positive	positive	high risk
STS10	mutagen	negative	positive	medium risk
STS11	mutagen	negative	negative	low risk
STS12	mutagen	negative	negative	medium risk
STS13	mutagen	negative	negative	medium risk
STS14	mutagen	negative	positive	high risk
STS15	mutagen	negative	positive	medium risk
STS16	mutagen	negative	negative	medium risk
STS17	mutagen	negative	positive	medium risk
STS18	mutagen	negative	negative	medium risk
STS19	mutagen	negative	positive	high risk
STS20	mutagen	negative	positive	medium risk
STS21	mutagen	negative	negative	low risk
STS22	mutagen	negative	positive	medium risk
STS23	mutagen	negative	negative	medium risk
STS24	Mutagen	negative	positive	high risk
STS25	mutagen	negative	positive	medium risk

Ames test-Ames test for mutagenicity in *Salmonella typhimurium*, **Carcinogenicity (Mouse)**-2 years carcinogenicity bioassay in mouse, **Carcinogenicity (Rat)**-2 years carcinogenicity bioassay in rat, **hERG Inhibition**-*In Vitro* Human Ether-a-go-go Related Gene Channel Inhibition

3.4. Summary

In summary, a library of 25 1,3,4-thiadiazole-2-amine derived thioacetamide derivatives (**STS series**) were designed by lead simplification of our in house lead compound **STT13** with an aim to improve the SHP2 inhibitory potential of the resultant scaffold. Essentially, the parent structure of compound **STT13** was shortened by envisaging better occupancy within the tunnel allosteric site of SHP2 and thereby better activity. The designed compounds were synthesized, characterized by FTIR, NMR and HRMS techniques and evaluated for SHP2 inhibition by the established fluorescence-based assay (**Figure 3.14**).

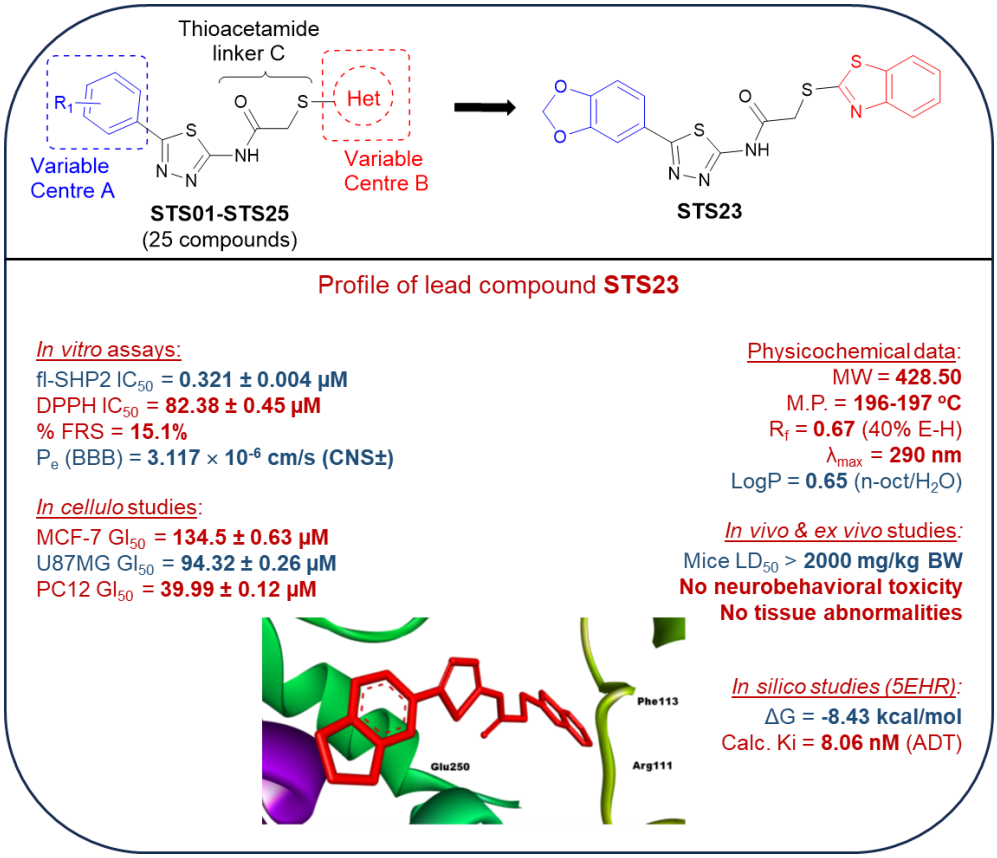

Figure 3.14. Summary of findings for the current series **STS01-STS25**

The molecule compound **STS23** (*N*-(5-(benzo[*d*][1,3]dioxol-5-yl)-1,3,4-thiadiazol-2-yl)-2-(benzo[*d*]thiazol-2-ylthio)acetamide) was the *in vitro* lead SHP2 inhibitor with an IC_{50} of 0.321 ± 0.004 µM. SAR study indicated that the benzothiazole derivatives were particularly potent against SHP2. *In silico* studies like molecular docking and MD simulation were carried out in the tunnel allosteric site of SHP2 to correlate the *in vitro* activity with the *in silico* interaction patterns of the molecule with SHP2. Few compounds of the series, when evaluated for their antioxidant activity by DPPH assay displayed moderate dose-independent antioxidant property. Cellular assays of compound **STS23** on MCF-7 cells revealed moderately potent antiproliferative, anti-survival and antimigratory effects. The molecule was found to be non-toxic up to a single oral dose of 2000 mg/kg BW in rats.